

Stimulation of 3D osteogenesis by mesenchymal stem cells via a nanovibrational bioreactor.

P. Monica Tsimbouri^{1†}, Peter G. Childs^{2†}, Gabriel D. Pemberton^{1†}, Jingli Yang¹, Vineetha Jayawarna¹, Wich Oripiriyakul¹, Karl Burgess³, Cristina Gonzalez-Garcia⁴, Gavin Blackburn³, Dilip Thomas⁵, Catalina V. Giraldo⁵, Manus J.P. Biggs⁵, Adam S.G. Curtis¹, Manuel Salmeron-Sanchez⁴, Stuart Reid^{2*#}, Matthew J. Dalby^{1*}

¹Centre for Cell Engineering, Institute for Molecular, Cell and Systems Biology, College of Medical, Veterinary and Life Sciences, University of Glasgow, Glasgow G12 8QQ, UK.

²SUPA, Institute of Thin Films, Sensors and Imaging, University of the West of Scotland, Paisley PA1 2BE, UK.

³Glasgow Polyomics facility, College of Medical, Veterinary and Life Sciences, University of Glasgow, Wolfson Wohl Cancer Research Centre, Garscube Campus, Bearsden, G61 1QH, UK.

⁴Microenvironments for Medicine, Division of Biomedical Engineering, School of Engineering, College of Science and Engineering, University of Glasgow, Glasgow, G12 8QQ, UK.

⁵Centre for Research in Medical Devices (CÚRAM), National University of Ireland Galway, Ireland.

[#]Now at SUPA, Department of Biomedical Engineering, Wolfson Centre, Strathclyde University, Glasgow, G4 0NW, UK.

†these authors contributed equally to this work

**corresponding authors* Stuart.Reid@strath.ac.uk and matthew.dalby@glasgow.ac.uk

Bone grafts are one of the most commonly transplanted tissues. However, autologous grafts are in short supply, and can be associated with pain and donor-site morbidity. The creation of tissue-engineered bone grafts could help to fulfil clinical demand and provide a crucial resource for drug screening. Here, we show that vibrations of nanoscale amplitude provided by a newly developed bioreactor can differentiate a potential autologous cell source, mesenchymal stem cells (MSCs), into mineralized tissue in 3D. We demonstrate that nanoscale mechanotransduction can stimulate osteogenesis independently of other environmental factors, such as matrix rigidity. We show this by generating mineralized matrix from MSCs seeded in collagen gels with stiffness an order of magnitude below those needed to induce bone formation *in vitro*. Our approach is scalable and can be compatible with 3D scaffolds.

With an aging population increasing the demand for musculoskeletal surgery, there is a growing need to provide viable bone grafts for clinical use¹. A wide range of surgeries require bone grafts², whose supply is limited³. Also, they are associated with donor-site morbidity⁴. Allogeneic decellularized grafts or synthetic ceramic alternatives, although widely accepted as substitutes, suffer from being biologically inferior *in vivo* relative to viable bone grafts^{1, 3}.

The creation of appropriate 3D bone mimics would also support a fail-fast, fail-cheap workflow for the pharmaceutical sector, allowing the rapid prioritization of the best candidates for *in vivo* or on-chip testing of drug leads⁵ for bone-related disorders, such as osteoporosis. A scalable method that does not require soluble factors or osteoinductive scaffolds to direct differentiation would be advantageous; it would prevent the confounding effects that arise from the use of differing media formulations or from the reliance on a limited selection of materials that are typically highly engineered⁶⁻¹³.

Tissue engineering provides a route to bioengineering bone-like environments, in which autologous cells with osteogenic potential, such as MSCs, are mineralized within a 3D scaffold using a bioreactor to aid *in vitro* tissue development. To achieve

cost-effective osteogenesis without the use of defined media or osteoinductive scaffolds requires a bioreactor that itself drives osteogenesis¹⁴; such a bioreactor would have implications for the pharmaceutical sector and the clinic¹⁵.

The designs of currently available bioreactors are complex, often involving unfamiliar and hard-to-use parts, such as rotary and perfusion chambers and associated tubing. The creation and use of these parts present major sterility, upscale and cost issues¹⁶. It would therefore be advantageous for a new bioreactor to be able to sit in a standard incubator, consist of a few parts, and to use off-the-shelf cell-culture containers that are easy to move between the bioreactor and a laminar-flow cabinet.

We have previously used nanoscale vibrational displacements to stimulate osteogenesis in MSCs cultured on tissue culture plastic in 2D^{17, 18}. This work identified that mechanical stimulation of 1000 Hz frequency with 15-nm vertical displacement promoted MSC differentiation¹⁸. The process was shown to be RhoA kinase (ROCK) dependent, consistent with known mechanisms of MSC osteogenesis in 2D cultures via increased adhesion-driven cytoskeletal tension¹⁸⁻²⁰.

Multi-sample nanovibrational bioreactor for 2D osteogenesis

In our previous 2D work¹⁸ only one sample could be stimulated at a time, and issues existed around vibration transmission, which meant that the nanovibrational setup was complex and lacked scalability. In our nanovibrational bioreactor, we employed a reverse piezo effect, where an applied voltage drives nanoscale displacements from piezo ceramics. The bioreactor design incorporates a 13-piezo array, mounted onto an aluminium base, directing expansion upwards (Figure 1a). Actuators can be wired in series or in parallel, with parallel wiring allowing higher vibration amplitudes to be produced. Mounted above the array is a top plate, which has a surface area capable of accommodating two 6-well culture plates. This plate is dual-layered, using aluminium bonded to magnetic stainless steel (Figure 1a). This design provides a balance of weight, rigidity, and the ability to magnetically couple 6-well plates via ferrite magnets attached to the base of each well. The magnets allow vibration to be

transferred to the 6-well plates, to provide extra rigidity to ensure the consistent transfer of vibration amplitude across each well, and to facilitate the removal of the plate when cells need to be fed.

When employing high-frequency vibration, it is important to consider the possibility of deformation. Using ANSYS finite element analysis (FEA), harmonic response models at 1000 Hz with 30 nm amplitude predicted: (1) that the bioreactor top plate would provide rigidity, minimizing average deformation at the nanometre level to ± 5 nm or 17% (Figure 1b); and (2) that the magnetic attachment of 6-well plates maintains amplitude accuracy across the growth surfaces (within 3.3 nm (11%) for frequencies <3600 Hz) (Figure 1c).

Laser interferometry techniques developed for gravitational wave research²¹ were used to validate FEA simulations. When wired in series, piezo actuators, without a top plate, gave an average vibration amplitude of 24.7 nm (8.3% accuracy between actuators - 1000 Hz, 80 Vpk-pk). Across 25 set points (Figure 1d), amplitude measurement of the top plate demonstrated the plate vibrated at 28.2 nm (11.2% amplitude consistency). Measurements made with the 6-well plates magnetically attached to the top plate (Figure 1d) revealed a slight reduction in displacement amplitude. However, displacement amplitude across multiple wells was shown to be consistent (21.2% accuracy in the range of 0-3000 Hz (Figure 1e)). Above 4000 Hz, the amplitudes increased towards a resonant condition (Figure 1e – denoted by large variance), as predicted by ANSYS (Figure 1c).

To confirm osteogenesis occurs in 2D, MSCs (from human bone marrow) were stimulated at 1000 Hz (80 Vpk-pk giving a 22 nm vertical displacement)¹⁸. While 1000 Hz may seem fast relative to the stimulation parameters employed with traditional mechanical bioreactors, it is noteworthy that for hydrated bone to be optimally piezoactive, a kilohertz range (972 Hz) stimulus is required²². Furthermore, research into the effects of nanotopography indicates that feature sizes of ~20 nm high are osteogenic^{23, 24}; this is very close to the 22 nm displacement we use here. After 7 days of MSC culture, quantitative (q)PCR was used to assess the expression of the osteospecific transcription factor, osterix, and significant up-regulation of its

expression was observed following nanostimulation (Figure 1f). Furthermore, levels of the proteins, alkaline phosphatase (ALP) at 14 days and osteopontin (OPN) at 21 days, were assessed in nanostimulated MSCs and compared to mature primary human osteoblasts using in-cell western analysis. Both the bioreactor-stimulated MSCs and the osteoblasts produced higher levels of these bone marker proteins relative to unstimulated MSCs (Figure 1g). These time points were chosen as they map onto classical osteodifferentiation progression models for transcription factors (osterix), early stage markers (ALP) and later stage markers (OPN)²⁵.

The 2D paradigm for osteogenesis^{19, 20, 26} indicates that adhesion-based signalling, including signalling via ROCK¹⁸, is important for nanovibration-induced MSC differentiation. However, in 3D systems, cellular mechanoreceptors might also play a role in MSC osteogenesis. Transient receptor potential (TRP) channels function as mechanosensors, and TRP channel activation occurs via cytoskeletal linkage²⁷. Two recently discovered mechanosensitive cation channels, called Piezo1 and Piezo2^{28, 29}, affect cytoskeletal organization^{30, 31} when mechanically activated, and render cells mechanosensitive to cell adhesion and/or cytoskeletal strain³². In non-excitabile (non-neural) cells, TRP and Piezo channels have been implicated in the transduction of vibrational force, for example in the stereocilia that signal changes in fluid pressure in the ear during hearing, indicating the sensitivity of these channels to high frequency vibration^{33, 34}. In addition, in a mouse model of osteoporosis, the depletion of the channel Trpv1 (TRP vallanoid sub-family 1)³⁵ protected mice against ovariectomy-induced bone loss³⁶.

A wide range of stimulus can activate TRP channels, including mechanical force, as long as the energy transduction to the channel is sufficient for mechanical gating to occur³⁷. Thus, we hypothesised a role for these channels in the response of MSCs to nanovibrational stimulation. Currently available inhibitors of Piezo1 (GsMTX4)³⁸ and of TRPV1 (QX314)³⁹, designed for studies of action potential, act transiently. Thus, to measure their effect on nanovibration-induced MSC differentiation, a very early stage marker of cell response was selected. Mitogen activated protein kinases, such as extracellular signal-related kinase 1/2 (ERK 1/2), provide a likely marker for the switch between MSC growth and osteogenic differentiation phases⁴⁰, with the onset of

differentiation typified by growth repression through high levels of ERK 1/2 activation (phosphorylation)⁴¹.

Using an MSC seeding protocol, which allows 1 hour for cell attachment in 10% serum, cells were both stimulated and synchronised at G0 by applying nanovibrations and serum starvation (1% serum) for 24 hours. After synchronising, cells were released back into the cell cycle using 10% serum for 23 hours before the addition of GsMTX4 or of QX314 for a further 1 hour (24 hours total). Active, phosphorylated, pERK1/2 was then assessed relative to total ERK1/2 protein levels using in-cell western analysis. The inhibition of both the Piezo1 and TRPV1 channels repressed ERK1/2 phosphorylation in the nanovibration-stimulated cells; no repression was seen in control cultures, suggesting that these changes were mechanotransduction-driven via Piezo1 and TRPV1 (Figure 1h). From these results, we hypothesised that channel-based mechanosensors might be important for the nano-mechanostimulation of MSCs in 3D.

Nanovibration in 3D gel volumes.

The ability to mechanically stimulate cells at the nanoscale in 3D is challenging because of the requirement to transmit nanoscale cues into 3D volumes. In order to test this, a 3D biocompatible scaffold that in itself should not initiate osteogenesis was used; collagen type I⁴². The gel was set at low elastic modulus as high-modulus gels can confer osteoinductive properties; ~40 kPa (notably the stiffness of pre-calcified bone matrix) has been shown to be osteoinductive to MSCs^{7, 26, 43-45}. Here, we used gels with a bulk elastic moduli of ~108 Pa without cells, and with a moduli of ~73.5 Pa at a loading density of 40,000 cells/ml of gel (Supplementary Table 1 and Figure 2a, 2b). Local elastic modulus (as a cell might sense it) was measured using AFM, and found to be ~59 Pa without cells and ~62 Pa with cells at a loading density of 40,000 cells/ml (Supplementary Fig 1).

To start to understand if collagen could transmit the nanovibrations, FEA harmonic response analysis was performed assuming that the ~108 Pa collagen gel was within the linear elastic range and incompressible (Poisson ratio $\nu = 0.5$)⁴⁶. For collagen gels

under strain, the Poisson ratio describes the absolute ratio between transverse and longitudinal strain. For this analysis, a Poisson ratio, ν , of less than 0.5 was chosen. Several values for ν were tested for their replication of the interferometric result with an asymptotic increase towards 0.5 improving the accuracy of the simulation (i.e. the ability to transmit a full vibration amplitude of 20 nm). The value used also resulted in a bulk modulus of the same magnitude as water (Supplementary Table 1). The bulk modulus describes a material's resistance to uniform compression; such materials tend to have a high water content, as in the case of collagen gels. Modelling of the polystyrene container showed it produced minimal deformation (Figure 2d). Modelling of the gel (at 2.5 ml of gel per well), at 1000 Hz with 20 nm displacement, predicted an average amplitude of 29 nm at the edge meniscus and 18 nm at the gel centre (Figure 2e).

Using these same modelling parameters, shear stress and strain within the gel produced peak values of 3.8 mPa and 1.1×10^{-4} m/m respectively at 1000 Hz (shear stress is shown in Figure 2f). These values fall within the linear region of the shear stress-strain plot in Figure 2c (from rheological measurement). This supports the validity of using a constant elastic modulus value for modelling nanovibration, at this frequency, since the strains produced are within the linear elastic range of the material. Hence, the viscoelastic properties of the collagen gel are predicted to allow the transfer of high frequency vibrations to the cells seeded in 3D.

Interferometry was again used to confirm predictions. The bioreactor was set up with a 6-well plate and with cells (40,000 MG63 cells/ml –note, MG63 cells were chosen as they can be used on the interferometer outside of the cell culture laboratory) seeded within 2.5 ml collagen gels. Measurements were carried out both at the centre and outer edge of the gels. Amplitude calibration showed that for the frequencies examined, gel vibration increased linearly with input voltage to the bioreactor (Figure 2h). In terms of frequency, the top surface of the gel was found to follow the surface of the 6-well plate consistently, showing no dampening of the vibration up to 2000 Hz. Gel samples that contained cells did not deviate in response from gels without cells (Figure 2i). Up to 2000 Hz, amplitude appeared to be increased at the edge of the gel at the meniscus curvature, thus reflecting the predicted data (Figure 1b). The vibration

amplitude seen at the edge of the gel was 35 nm compared to 24 nm at the centre for 1000 Hz (Figure 2i – inset).

Resonant frequencies were recorded in the region of 2500, 3500 and 5000 Hz and were observed in both empty and gel-filled 6-well plates. We also observed an increase in vibration amplitude at the outer edge of each well when compared to its centre, together with a decrease in measurement accuracy (Figure 2i). If the gel volume is doubled to 5 ml, the data indicate that a slight amplitude-dampening effect occurs, although the gels act similarly in terms of where resonance occurs with different voltage input, and with respect to middle/edge amplitude changes (Supplementary Figure 2). Our results also indicate that cells within the ~100 Pa gels should receive predictable and reproducible nanoscale displacements. However, this gel environment is dramatically different to the hard environment of the plastic cell culture well (as used to generate Figure 1f & g) or to 40 kPa gels, which have previously been used to stimulate osteogenesis^{7, 26}, and this presents a significant challenge in terms of achieving osteogenesis.

Nanovibration driven 3D osteogenesis.

To test MSCs for osteogenesis in the ~108 Pa collagen gels, a range of viability and osteo-specific transcriptional, protein and mineralisation assays were performed. In terms of viability, our analysis showed that MSCs embedded in these gels (referred to hereafter as 3D) remain viable during nanostimulation (Supplementary Figure 3). To assay for osteogenesis, qPCR at days 7, 14 and 21 of culture was performed, and showed increased RUNX2, collagen I, ALP, OPN, osteocalcin (OCN) and bone morphogenetic protein 2 (BMP2) expression in the nanostimulated MSCs in 3D, compared to unstimulated MSCs (Figure 3a). In MSCs that were nanostimulated, four of the six genes above were downregulated at day 21, as the osteogenic process was transcriptionally completed (Figure 3a). OCN protein levels were also assayed at day 21 and found to be increased following nanostimulation demonstrating progression from gene to protein (Supplementary Figure 4).

To study *in vitro* mineralisation, we used a combination of von Kossa staining for phosphate, Raman spectroscopy, and X-ray micro-computed tomography (μ CT). Von Kossa staining indicated that relatively little mineralisation had taken place within control gels (Figure 3b – images are from 6 weeks of culture). However, following nanostimulation at 15 nm displacement, significant mineralisation was detected in MSCs cultured in 3D. Mineralisation levels were higher in these cells than in MSCs after 4 weeks of culture in osteospecific media (OSM) (Figure 3b). In longer-term, 6 week, culture, MSCs cultured in 3D with OSM caught up and underwent a significant increase in mineralisation compared to control cells (Figure 3b).

Within the Raman fingerprint region of 500 to 1500 cm^{-1} (Figure 3c,d,f and Supplementary Figure 5), bovine cortical bone showed a dominant phosphate (PO_4^{3-} ν_1) peak at 960 cm^{-1} and a secondary peak at 1072 cm^{-1} , characteristic of substituted carbonate (CO_3^{2-}) and indicative of the mineral component of bone⁴⁷, as well as of hydroxyapatite $\text{Ca}_{10}(\text{PO}_4)_6(\text{OH})_2$, where CO_3^{2-} can substitute for OH^- and/or PO_4^{3-} (Figure 3c). For MSCs cultured in control gels, a broad, merged peak from 1200 cm^{-1} was observed (likely due to the large amount of collagen present), and protein-related contributions from amide I (1595-1720 cm^{-1}) and III (1243 -1269 cm^{-1}) and from CH_2 (1451 cm^{-1}). Significantly, no bone mineral peaks were noted in these cells (Figure 3d) and μ CT revealed no mineral deposits (Figure 3e). In nanostimulated MSCs in 3D, two peaks at 960 cm^{-1} (PO_4^{3-} ν_1) and 1072 cm^{-1} (CO_3^{2-}) were observed (Figure 3f), and μ CT showed the accumulation of bone mineral (Figure 3g, Supplementary Table 2). Together, these findings demonstrate that nanostimulation can drive osteogenesis and mineralisation in MSCs in an otherwise non-osteogenic 3D environment.

3D nanovibrational stimulus of mechanosensitive channels.

We next tested ion channel sensitivity to 3D nanostimulation in order to relate ion channel expression to cytoskeletal tension. Temporal qPCR was performed on MSCs at days 3, 5, 7, 14 and 21 of culture to assay the expression of Piezo 1, Piezo 2, TRPV1 and of potassium channel subfamily K receptor 2 (KCNK2, which is stimulated by membrane stretch⁴⁸). Nanostimulation of MSCs in 3D produced a similar trend across

all the channels tested, specifically a bi-phasic high to low expression pattern from day 3 to day 5, recovery to a higher level at days 7-14 to a lowered expression pattern at day 21, with all channel transcripts significantly downregulated by day 21, post-osteogenesis (Figure 4a). From our 2D data¹⁸ and from the literature on osteospecific differentiation on a range of 2D surfaces^{19, 20}, it could be postulated that intracellular tension should increase during osteogenesis; thus, if the channels were involved in osteogenesis in 3D, they might be sensitive to tension inhibitors, such as the ROCK inhibitor (Y27632) and the myosin II inhibitor (blebbistatin).

To test this hypothesis, day 5 was selected as a representative time point for the downregulation of Piezo 1, Piezo 2 and TRPV1 channel expression (Figure 4a) and, as we were now investigating a single time point, MSCs from additional donors were supplemented into the analysis. All three ion channels were downregulated by day 5, with Piezo 2 being significantly down-regulated. The trend was noted in OSM-treated cells, but was more pronounced in MSCs subjected to nanostimulation (Figure 4b-e). Upon addition of Y27632 and blebbistatin, the down-regulation of Piezo 2 expression was reversed, indicating a relationship exists between this receptor and cellular tension. This trend was noted in both nanostimulated and OSM-treated cells, but was more pronounced following nanostimulation (Figure 4c). TRPV1 also showed a tension-dependant link, increasing in expression with nanostimulation and OSM treatment following treatment with Y27632. Again, this was more pronounced for nanostimulated cells, as blebbistatin treatment increased the expression of TRPV1 only in nanostimulated MSCs (Figure 4e).

The effect of actin and ROCK inhibition on early stage (to day 5) osteogenic transcripts was next investigated in nanostimulated MSCs. BMP2 receptor (BMPRIa) was differentially regulated in blebbistatin-inhibited MSCs (Figure 4f). The response to BMP2 is a first step in osteogenesis and it stimulates transcription factors, such as RUNX2 (the master osteogenic transcription factor, which peaks in expression at day 5-10)²⁵. At this early time point, however, RUNX2 expression was not altered in response to either inhibitor (Figure 4g). ALP, a later stage marker of osteogenesis (which peaks in expression ~day 14^{25, 49}), was minimally expressed (Figure 4). At day

14, blebbistatin treatment downregulated the expression of two later stage markers of osteogenesis, osteonectin (ONN) and OPN (Supplementary Figure 6).

These data support the hypothesis that 3D osteogenesis *via* nanovibrational stimulation is a mechanotransductive process that involves intracellular tension, with mechanoreceptors, such as Piezo, TRP and KCNK, being involved in this process. However, we note that our results are not as dramatic, in terms of response to cytoskeletal inhibition, as seen in 2D osteogenesis studies^{19, 20, 26}.

Nanovibrational mechanotransductive signalling.

The receptor that appeared most mechanoresponsive to nanostimulation at this timepoint (day 5) was TRPV1. It has been proposed that TRPV channels influence osteogenesis through the β -catenin (Wnt pathway) activation of RUNX2^{50, 51}. In this pathway, ion influx through the TRPV channels causes the activation of protein kinase C (PKC) and of ERK, mediating β -catenin activity^{50, 51}.

To investigate the effects of nanovibrations on signalling processes in MSCs, we used metabolomic analysis to predict canonical signalling events as this approach provides an instant picture of phenotypic modulation. Principle component analysis showed that 3D nanovibrated MSCs and control MSCs, had different metabolomes indicative of different phenotypes (Supplementary Figure 7a). As expected during active differentiation, energy based pathways⁵² were upregulated in nanostimulated MSCs, including lipid (Supplementary Figure 8) and carbohydrate (Supplementary Figure 9) metabolic pathways, with lipids representing the largest group. Ingenuity pathway analysis (IPA) fits metabolite input data to the literature in order to be able to predict biochemical interactions. It was used here to build networks related to lipid metabolism, that were merged and linked to canonical signalling pathways related to adhesion, cytoskeletal tension, ERK 1/2 signalling, BMP2 signalling and calcium/Wnt signalling^{19, 20, 26} (Supplementary Figure 7b).

To investigate if TRPV plays a role in the osteogenic process, western blot densitometry was used to measure key members of these pathways after control and

nanovibrational culture. Specifically, pFAK, pMyosin, pERK, pSMAD1/5/8 and active β -catenin, with and without inhibition of PKC with enzastaurin, were considered. Only β -catenin was affected, becoming down-regulated as PKC was inhibited and the normal functioning of TRPV channels was indirectly blocked (Figure 5a – no effect of PKC inhibition was seen in 3D MSCs treated with OSM, Supplementary Figure 10).

We next investigated the effect of channel inhibitors on nanostimulated MSCs in 3D by measuring total ERK 1/2 and total β -catenin levels in the presence and absence of PKC and TRPV channel inhibition. MSCs in 3D underwent nanostimulation (1000 Hz), nanostimulation with PKC inhibition (1000 Hz-PKC), and nanostimulation with TRPV inhibition (1000 Hz-TRPV); protein levels were assayed after 48 hours of stimulation (Supplementary Figure 11). At the same time, a metabolomics/IPA analysis was performed to investigate signalling networks linked to the β -catenin/Wnt pathways. Western blot analysis showed that nanostimulated MSCs treated with PKC and TRPV inhibitors downregulated the expression of ERK 1/2 and β -catenin but that only β -catenin was significantly down-regulated in the presence of both inhibitors (Figure 5b). The metabolomics analyses indicated that the Wnt/ β -catenin pathway was upregulated following nanostimulation (Figure 6a), but was moderately down-regulated in the 1000 Hz-PKC MSCs (Figure 6b) and largely suppressed in the 1000 Hz-TRPV cells (Figure 6c) (see Supplementary Figures 12-14 for more complete networks). The metabolomics analysis also inferred that ERK signalling is downregulated in the 1000 Hz-PKC and 1000 Hz-TRPV MSCs (Figure 6a-c), which is in agreement with the western blot data which show that total ERK protein levels are reduced (Figure 5b). Together, these findings lead us to propose that TRPV1 activity contributes to Wnt-mediated osteogenesis in nanovibrated MSCs in 3D. Potential mechanisms are shown in Figure 6d with the TRPV/ β -catenin pathway highlighted in bold.

To test if inhibition of PKC and TRPV have direct effects on osteogenesis in 3D culture, nanovibrational stimulation time was extended out to 5 days to allow for some phenotypical development and the cultures were inhibited for PKC or TRPV for the final 24 hours. QPCR was used to test transcript level changes; we looked at BMPR1a and BMP2 as very early markers, RUNX2 as an early marker and ALP and osteonectin

as mid-stage osteogenic markers. For PKC inhibition, downregulation of BMP2 was observed indicating a phenotypical response (Figure 7). However, with TRPV inhibition, significant downregulation of BMP2, RUNX2, ALP and osteonectin was observed showing an immediate and dramatic effect on progression of the osteogenic phenotype. This data supports that TRPV channels are important to osteogenesis and that PKC may also have effect (but indicating that it might not be an exclusive effect), helping build the hypothesis presented in Figure 6d.

We have presented a new class of bioreactor and showed that 3D osteogenesis can be produced without the use of chemicals and/or growth factors, or of bioactive scaffolds, sophisticated culture ware, or dedicated incubators. The use of collagen in this study provided mechanical integration with the 6-well plate because it attaches to the dish sides. This allowed us to take advantage of its excellent mass-transfer properties, which also permit large volumes to be used, avoiding the need to use dense osteogenic scaffolds, such as calcium phosphates and other bioactive ceramics, which have certain disadvantage and limitations. In fact, on a single bioreactor with 5 ml of gel fill per well, 60 ml of mineralising osteoblasts in an appropriate 3D matrix can be generated from MSCs.

Summary.

In addition to the potential volumes of graft material that could be produced using this bioreactor, it also fits well into a good-manufacturing-practice (GMP) workflow. GMP-grade collagen, media and culture plates exist and have been used in human trials⁵³. In this approach, the nanovibrational bioreactor remains external to these components as it does not come into contact with cell-therapy products. This prevents the need to, for example, meet FDA regulation for new scaffolds or induction chemicals.

We propose that, because of the soft 3D nature of the collagen matrix used in our approach, the magnitudes of the roles for adhesion and cytoskeletal tension were lower than those observed in 2D studies^{19, 20, 26}. We also suggest an increased role for

mechanoresponsive channels, which we believe stimulate enhanced osteogenesis through the activation of β -catenin signalling.

Acknowledgements. This work was supported by grants to Reid and Dalby from BB/N012690/1, BB/P00220X/1, EP/N013905/1, EP/N012631/1, EP/P001114/1 from BBSRC, BBSRC/SFI and EPSRC and a programme grant from Find a Better Way. We thank Jim Hough, Habib Nikukar, Ivor Tifenbrun and Keith Robertson for their discussion, Carol-Anne Smith for technical support, and Erin Manson for help with metabolite analysis. Biggs is funded by SFI grant nos. 11/SIRG/B2135 and 13/RC/2073.

Author Contributions. *PMT, PGC, GDP, JY, VJ, WO, CG-G, DT and CVG performed the laboratory experiments. PMT, PGC, GDP, WO, KB, GB, MJPB, MSS, SR and MJD analysed the data. PMT, PGC, GDP, MJPB, ASGC, MSS, SR and MJD devised experiments. SR and MJD supervised the research. PMT, PGC, GDP, MSS, SR and MJD wrote the manuscript. PMT, PGC, SR and MJD revised the manuscript.*

Competing Interests. *The authors declare no competing financial interests*

Materials & Methods

Vibration apparatus. The bioreactor surface area was designed to hold two 6-well plates (Corning, NY) simultaneously with dimensions of 130 × 178 mm. The piezo actuators used (PL088.30, Physik Instrumente, Karlsruhe, Germany) were low profile actuators with a large attachment area. The top plate of the platform utilised magnetic attachment to secure the 6-well plates. Standard 30 mm diameter, 3 mm thickness Fe₂O₃ ferrite magnets (Magnet Expert, Tuxford, UK) were bonded to the tissue culture plates. The quoted magnetic flux at the surface of these magnets is 700 gauss (0.07 T) which as a static magnetic field is not thought to be high enough to alter cellular function. However, these magnets, being halbach arrays, are only magnetic on the side facing the bioreactor and away from the cell culture therefore any stray magnetic fields will be far smaller.

To power the piezo array, a high voltage piezo driver (Model ENV 150, Piezosystem Jena, Jena, Germany) was used which is capable of providing 160 V_{pk-pk}. The sine wave modulation of the amplifier output was provided by a signal generator (Model 33210A, Agilent, Santa Clara, CA).

Finite element modelling (ANSYS). Simulated models of a Corning 6-well plate, the bioreactor top plate and the collagen gel were developed in ANSYS finite element software (ANSYS, Canonsburg, PA). Models were developed in ANSYS Workbench v14.0 with analysis involving use of the Harmonic Response package to provide values for deformation at user defined frequencies.

The culture plate component was modelled as a polystyrene plate bonded to six ferrite magnets via a 0.2 mm layer of epoxy. A similar method was used to model the top plate with materials bonded with a 0.1 mm epoxy bond. Epoxy bonds were also added at the attachment points of the piezo actuators. For this analysis, vibration frequencies of 0 to 10,000 Hz, with 30 nm amplitude, were applied to the models to compare amplitude consistency. Throughout all the analysis, mesh relevance was set at 0 giving a medium mesh density.

For studies of the collagen gel, the model incorporated the polystyrene culture ware (one well of a 6-well plate, and bonding to the vibration source through a 0.1 mm epoxy layer. Harmonic response analysis was used to study the frequency dependant effects of deformation of the gel construct including meniscus curvature at the edge (modelled using the linear shear moduli and assumption of incompressibility) along with estimates of the levels of shear stress within the construct. Vibration condition was set to 1000 Hz, 20 nm, to model the frequency used in experiment. Harmonic response analysis is strictly linear so accuracy would be limited to the linear elastic range of the material. However, the modelled values for shear stress fall within the linear elastic range measured through rheology suggesting this is an accurate modelling assumption for nanoscale vibration. Mesh sizing was set to coarse to reduce computational time. Connections between the gel and the culture ware were set to bonded (assuming that the gel adheres to the culture ware) and used multi point constraints (MPC) to ensure that the mesh was constrained to the container. The additional impact of gravity was incorporated through an inertial acceleration of 9.81 ms⁻¹.

Interferometric measurement. Assessment of vibration amplitude was carried out using laser interferometry. A USB interferometer (Model SP-S, SIOS Meßtechnik GmbH, Ilmenau, Germany) was mounted on a frame with the laser aimed downwards at the measurement site. In the case of the rigid culture surface, silicon fragments were bonded at measurement sites to reflect the laser and for collagen measurements, 50 µm thickness silicon fragments were used to minimise any effect from the weight of the fragment. The interference condition of the reflected light is processed and passed to INFAS analysis software where a Fast Fourier Transform (FFT) produces a frequency spectrum for displacement. This model of interferometer is sensitive to displacements of 0.1 nm however at low frequencies the limitations of the system are actually due to background motion. For each measurement, a value for background noise at that frequency was recorded. To partially reduce the effect of

this noise the interferometric apparatus was sat on a rubber mat to provide a partial noise dampening.

Rheology. Assessment of the physio-elastic properties of the collagen matrix was performed by carrying out dynamic frequency sweep experimentation. These frequency sweeps were performed by using a strain-controlled rheometer (Kinexus rotational rheometer system, Malvern Instruments, Malvern, UK). The parallel-plate used to perform the frequency sweep had a 20 mm diameter with a 0.25 mm gap. An integrated thermostat mechanism was used to maintain the sample temperature at 25°C. In order to keep the sample hydrated and prevent drying out through evaporation the internal atmosphere was kept saturated through the use of a solvent trap. An amplitude sweep was carried out and this confirmed no variation in elastic modulus (G') and viscous modulus (G''). The amplitude sweep was performed up to a strain of 1% and these measurements were taken in a linear viscoelastic regime. The collagen matrix dynamic shear modulus was measured as a frequency function with a frequency range from 1 to 100 Hz. To ensure reproducibility all measurements per sample were performed in triplicates.

Characterisation of collagen matrices by AFM. The fibrillar conformation of type I collagen gel matrices was assessed via AFM in AC mode (Nanowizard 3 Bioscience AFM, JPK Instruments AG, Berlin, Germany). Collagen gel (2 mg/ml) was gently dried with a nitrogen flow before evaluation in the AFM working in air. A pyramidal silicon nitride tip, with a cantilever spring constant of ~ 3 N/m and a resonance frequency of 75 kHz (MPP-21120, Bruker), was used to scan the collagen matrix. Height and phase images were simultaneously recorded. The influence of cell seeding density in the local mechanical properties of the collagen gel matrices was evaluated via force spectroscopy. Silicon tipless cantilevers (Arrow TL1, Nanoworld) functionalised with 20 μm silicon beads were used to perform the measurements. Force-distance curves were obtained, after calibration of tip sensitivity and spring constant, with a set-point of 10 nN, a zeta length of 10 μm , a constant duration of 1 s, and at room temperature in liquid environment. Analysis was performed using the JPK processing software (v4.3.21), and force curves were fitted with a Hertz model.

Cell Culture and collagen gel sample preparation. Primary bone marrow MSCs were sourced (Promocell, Heidelberg, Germany) and MG63s were taken from a cell line (ATCC, Manassas, USA). For critical experiments, cells from more than one donor were used and this is indicated in the figure legends and in Supplementary Table 5. We further note that over this study, MSCs from more than 20 donors were used. Cell concentration was typically 40,000 cells/ml (or 100,000 cells per 2.5ml collagen gel). Expanded MSCs were used at passages 1-3. The basal media that was used to maintain both cell types during experiments and for proliferation was DMEM (Sigma-Aldrich, St. Louis, USA) supplemented with 10% FBS (Sigma), 1% sodium pyruvate (11 mg/ml, Sigma), 1% Gibco MEM NEAA (amino acids, Thermo Fisher Scientific, Waltham, USA) and 2% antibiotics (6.74 U/mL penicillin-streptomycin, 0.2 $\mu\text{g}/\text{mL}$ fungizone). Before use, cells were trypsinised and counted with a haemocytometer. MSCs were homogeneously seeded within a collagen matrix a population of 4×10^4 cells/ml of gel.

All cell culture was performed in an incubator at 37°C with 5% CO₂. The basal culture media was removed and replenished every 2-3 days. For the osteospecific media positive control samples the DMEM basal media was also substituted with 100 µMol ascorbic acid and 50 nMol dexamethasone (Sigma) (OSM). The collagen matrix was prepared by addition of 10x modified eagle's media (Sigma), FBS, basal media with the appropriate number of cells and 2.05 mg/mL rat tail Type I collagen (First Link UK, Wolverhampton, UK) in 0.16% acetic acid. The solution was homogeneously mixed by pipetting. Following this 0.1 M NaOH was added while on ice, until a permanent pink/red colour change (phenol red indicator) was observed, to form a gel. The samples were then quickly placed in a 37°C incubator avoiding agitation.

Alamar blue assay. 4 × 10⁴ MSCs/ml of gel (2.5 ml) were stimulated at 1000 Hz. The Alamar blue assay was performed after 1 and 2 weeks of stimulation and compared to non-stimulated controls. Cultured media was removed and hydrogels were washed 3x in warm 1xPBS. 10% (v/v) of AlamarBlue[®] resazurin (Bio-Rad, Watford, UK) diluted in phenol-red free media (D5030, Sigma) was added to each hydrogel. After further incubation for five hours at 37°C, 5% CO₂, the culture supernatant was transferred into 96 well plates to measure the up-taken Alamar blue indicating cell metabolism. A microplate reader (Clariostar, BMG Labtech, Germany) was used to detect light absorbance at wavelengths of 570 nm and 600 nm. The percentage of Alamar blue reduction was calculated as following;

$$\% \text{ of reduction of Alamar}^{\text{®}} \text{ blue} = \frac{(O2 \times A1) - (O1 \times A2)}{(R1 \times N1) - (R2 \times N1)} \times 100$$

O 1 = molar extinction coefficient of oxidized Alamar blue at wavelength 570 nm.

O 2 = molar extinction coefficient of oxidized Alamar blue at wavelength 600 nm.

R 1 = molar extinction coefficient of reduced Alamar blue at wavelength 570 nm.

R 2 = molar extinction coefficient of reduced Alamar blue at wavelength 600 nm.

A 1 = Observed absorbance reading for test wells at wavelength 570 nm.

A 2 = Observed absorbance reading for test wells at wavelength 600 nm.

N 1 = Observed absorbance reading for negative control wells at wavelength 570 nm.

N 2 = Observed absorbance reading for negative control wells at wavelength 600 nm.

Live-dead staining. 4×10⁴ MCSs/ml of gel (2.5 ml) were seeded in each well of a 6 well plate for stimulated and control groups. MSCs were nanovibrated at 1,000 Hz for 2 weeks. Upon completion, the culture medium was removed and the samples were washed 3x in warm 1xPBS. 4 mM of calcein AM (Life Technologies, Carlsbad, USA) and 2mM of ethidium homodimer-1 (Life Technologies) diluted 1:1000 in phenol-red free media (D5030, Sigma) was added in each well. The samples were then re-incubated at 37°C, 5% CO₂ for 2 hours. 10x magnification microscopic images were taken (Olympus, Pennsylvania, US) operated on Surveyor software version 9.0.1.4 (Objective Imaging, Cambridge, UK). FITC/TRITC channel images were stitched and processed using ImageJ (Version 1.50g, National Institutes of Health, USA) and Photoshop CS4 (version 11 extended, Adobe, Ireland).

Cytoskeletal inhibition in 3D. MSCs were seeded at 4×10^4 cells/ml of gel (2.5 ml) in stimulated and control culture for 5 days in the presence or absence of inhibitors of ROCK (Y27632, Sigma) at 10 μ M and myosin II (blebbistatin, Sigma cat: B0560) 50mM. Inhibitors were added fresh with all medium changes for the duration of the experiment.

Transient receptor potential (TRP) channel inhibition in 2D. 1×10^4 MSC cells/well were cultured in 24 well plates for 1 hour with 10% serum for cell attachment and followed by serum starvation (1% serum) for 24 hours to synchronise the cells in G0. After synchronising, fresh basal media was added to cells to start the cell cycle and nanovibration stimulation was simultaneously applied for 23 hours (no stimulation in the control samples) before addition of inhibitors (GsMTX4 (for Piezo1, 4 μ M Tocris Bioscience cat: 4912,) and QX314 (Sigma cat: L1663) for TRPV1, 1% (v/v) of a 50 mg/ml stock) for the last 1 hour (24 hours total).

Transient receptor potential (TRP) channel inhibition in 3D. Serum starved MSCs seeded at 4×10^4 cells/ml of gel (2.5 ml) in stimulated and control cultures were cultured for 2 or 5 days in basal medium. For the last 24 hours QX314 (Sigma cat: L1663) was added at 8-hour intervals at 1% (v/v) of a 50 mg/ml stock) concentration. Samples were then processed for either protein or gene expression according to the methods provided.

PKC inhibition in 3D. *Method 1 for 5 day culture:* MSCs seeded at 4×10^4 cells/ml of gel (2.5 ml) in stimulated and control 6 well plates for 5 days in the presence of enzastaurin (Tocris Bioscience cat: 5994), a PKC inhibitor. The inhibitor was used at 1 μ M concentration for the duration of the experiment. *Method 2 for 2 or 5 day culture alongside TRPV inhibition:* serum starved MSCs seeded at 4×10^4 cells/ml of gel (2.5 ml) in stimulated and control conditions were cultured for 2 or 5 days in basal medium. For the last 24 hours enzastaurin was added at 8-hour intervals at 1 μ M concentration. Samples were then processed for either protein expression, gene expression or metabolomics analysis according to the relevant methods.

In-Cell Western Assay. MSCs within the 6 well (3D, 4×10^4 cells/ml of gel) or 24 well plates (1×10^4 cells) were fixed using 10% formaldehyde for 15 min. The cells were then permeabilized and blocked using 0.5% milk protein in 1xPBS-0.1%Tween20 (v/v) (PBST). All antibodies were diluted in 0.5% milk protein in PBST. GAPDH and CellTag 700 stain (Li-COR, cat: 926-41090, Lincoln, USA) were used as the reference controls. CellTag or rabbit anti-GAPDH primary antibody was diluted at 1:2000. Primary antibodies for target proteins ALP (Abcam, cat: ab354, Cambridge, UK), OCN and OPN (Santa Cruz Biotechnology, Cat:Sc-21742, Dallas, USA), phosphoERK (Cell signaling, Cat:4797s) and total ERK (Cell Signaling Technology, Cat:4696s, Danvers, USA) were then prepared in a dilution of 1:200. The primary antibody incubation was carried out at 37 $^{\circ}$ C for 2.5 hours, following 5 washes in PBS/0.1% Tween. The washes were carried out with agitation for 5 minutes. For CellTag as reference control, the Li-COR secondary antibodies (anti-rabbit, cat: 926-32211; anti-mouse, cat: 926-32210) were used at a dilution of 1:2000. For GAPDH as reference control, the secondary antibody was

diluted at a dilution of 1:5000 with a 680 nm infrared dye and GAPDH secondary antibody (donkey anti-rabbit) also had a dilution of 1:5000 with an 800 nm infrared dye. The secondary antibodies were incubated at ambient room temperature on a shaker for 1.5 hour, followed by 5x5min washes in PBS/0.2% Tween. The quantitative spectroscopic analysis was carried out using the LI-COR Odyssey Sa and all dyes and secondary antibodies were sourced from LI-COR corporation.

Quantitative Reverse Transcription polymerase chain reaction (QPCR). Following the required period of stimulation (3, 5, 7, 14, 21 days) within the bioreactor, the MSCs in collagen gels were assessed by qRT-PCR. Nanovibrated and control samples were extracted at the same time. The collagen matrix samples were removed from the 6 well plates and placed in a 15ml Falcon tube. Equal volumes of Trizol reagent (Life Technologies) was added to each sample, which were then vortexed and homogenised using a syringe with 20-G needles. 0.2ml of chloroform (Sigma) was added per ml of Trizol to each sample, mixed and centrifuged in order to separate the aqueous and organic phases. The aqueous phase was removed and the total RNA content was then extracted using the Qiagen RNeasy extraction kit (including a DNase step) according to the manufacturers instructions (Qiagen, Hilden, Germany). The RNA concentration was quantified using Nanodrop, and normalized for each sample. cDNA was prepared by reverse transcription using the Qiagen Quantitect kit. 12 μ L of the normalised dilutions for each RNA sample were added to a 0.2 mL (200 μ L) reverse transcription PCR – Cup. To each of the samples 2 μ L gDNA wipeout buffer was added. Following this each sample was run at 42°C for 2 mins, on a thermal Cycler (PCR) system in order to remove any DNA present in the samples. Following the removal of the innate DNA, 6 μ L of a stock solution (containing Qiagen reverse transcription buffer reagents) was then added to each reverse transcription cup, to give a total volume of 20 μ L. The second program (Supplementary Table 3) was then initiated to reverse transcribe the RNA into cDNA which was subsequently used to perform PCR quantification using the relative comparable method. The Quantifast SYBR green qPCR kit (Qiagen) was used to perform amplification with specific primers (Eurofins Genomics, Ebersberg, Germany) related to osteogenesis as well as GAPDH, ACTIN and 18s which were used as a genetic internal controls, listed in (Supplementary Table 4). PCR was quantified using the $2^{-\Delta\Delta C_t}$ method and amplification was carried out using an Applied Biosystems 7500 Real Time PCR system. Unstimulated samples also cultured in a 3D collagen matrix (samples not nanovibrated) were used as negative controls for comparison of osteogenic transcription expression.

Western blotting. Following the required period of stimulation within the bioreactor (2 or 5 days experiments) MSC protein expression was assessed (4 replicas per patient sample was pooled together for loading on to gels) at a density 4×10^4 cells/ml of gel (2.5 ml). MSCs were extracted from the collagen gels using collagenase D (Roche, UK) at 2.5 mg/ml. The gels were incubated in the collagenase solution for 90min at 37°C, transferred in a universal tube and cells pelleted at 1400rpm for 4min. The cells pellets were lysed directly by using protein lysis buffer (20 mM Tris–HCl, pH 7.5, 150 mM NaCl, 1 mM EDTA, 1% v/v Triton X-100) containing phosphatase and protease inhibitors (complete ULTRA Tablets, Mini, EASYpack no. 05892970001, and PhosSTOP phosphatase inhibitor cocktail tablets no. 04906845001, Roche). Protein

concentration was determined using the Nanodrop. Protein samples were run on a pre-cast NOVEX gradient (4-12%) gel system (Invitrogen, Thermo Fisher) and the samples were then transferred onto nylon membrane (Imobilon F, Millipore suitable for use with the Li-COR Odyssey system) according to manufacturer's protocol. For probing, the blots were incubated in 5% BSA TBS 0.1% (v/v) Tween 20 with the appropriate anti-sera dilution. Antibodies (1:1000 dilution in 5% BSA/0.1% TBST) used were directed to: phosphoERK (Cell Signaling, Cat:4797s) and total ERK (Cell Signaling, Cat:4696s), p-myosin (Cell Signaling, phospho Ser 19, no. 3675), total myosin (Cell Signaling, cat:3672s), beta catenin (anti-active β -catenin, clone 8E7, cat:05-665 and anti- β -catenin, clone 7F7.2, cat:04-958, Millipore, Billerica, USA), phospho SMAD1/5/8 (S463/465, Cell Signaling, cat:6944s) and total SMAD1 (Cell Signaling), pFAK (Y925) (Cell signaling, cat:3284P) and total FAK (MBL Life Sciences, cat:D061-3, Aichi, Japan), and total TRPV1 (Abcam, cat:ab111973) were then prepared in a dilution of 1:200. The primary antibody incubation was carried out at 4°C overnight for the phosphorylated proteins and at room temperature for 1-2 hours for the total proteins, followed by 3x5min washes in 0.1% TBST on a shaker. For the Li-COR secondary antibodies (anti-rabbit, cat: 926-32211; anti-mouse, cat: 926-32210) were used at a dilution of 1:8000. The secondary antibodies were incubated at ambient room temperature on a shaker for 1hour, following 3 washes in 0.1% TBST, again with agitation for 5 minutes. Total protein was measured using the Revert total protein stain (Li-COR) solution and used as loading control to normalize the samples where necessary. The quantitative spectroscopic analysis was carried out using the LI-COR Odyssey Sa and all dyes and secondary antibodies were sourced from LI-COR corporate.

Raman Spectroscopy. The 3D collagen gel matrix samples were nanovibrated for 46 days, were partially dried and were directly assessed by Raman spectroscopy without further sample preparation. 4×10^4 MSCs/ml of gel (2.5 ml) were seeded in each well. A Renishaw InVia Raman spectrometer with a 785 nm line focus laser was used to perform near IR spectroscopic scans. A reference standard of bovine cortical compact bone was used to assess the predominant finger print region spectrum for perfectly mineralised bone, and it was determined that 960 cm^{-1} and 1170 cm^{-1} were the predominant scattering wavenumbers. A light microscope (Leica, Wetzlar, Germany) x20 magnification was used to determine regions of interest and mineral deposition for assessment.

Von Kossa Staining. Nanovibrated 3D collagen matrix samples were stimulated for 4 or 6 weeks and were then fixed using 10% formaldehyde at 37°C for 30 minutes. Each well was seeded with approximately 4×10^4 cells/ml of gel (2.5 ml). The matrix samples were then submerged in 5 % silver nitrate and exposed to UV lamp for approximately 30 minutes. The samples were washed 5 times in deionized water and were then submerged in 5% sodium thiosulphate for 10 minutes so as to remove any excess silver nitrate. The samples were rinsed 5 times with agitation in deionized water, followed by 70% ethanol/30% water. The samples were then imaged without further preparation and the staining intensities were quantified using image J.

Micro-CT (μ CT) Analysis. MSCs were nanovibrated in 3D at 1000 Hz in a collagen gel extracellular matrix for 35 days the samples were fixed using 10% formaldehyde and

transferred into PBS and subsequently imaged using μ CT. The scans were then compared against unstimulated controls. For this experiment, each well (of the 6 well plate) was seeded with 750,000 cells per 2.5 ml gel. In order to image the samples all the gels for both the test sample (stimulated at 1000 Hz) and controls were combined together in a separate cryo tube manufactured by Nunc A/S, with an internal diameter of 9.8 mm (\pm 0.1 mm). Within the cryo tube the polystyrene saturated with PBS was used to secure the gels in place. This ensured that the samples were unable to move during scanning. Polystyrene was utilized as it is radiolucent and allowed the gels to be imaged unobstructed. The μ CT system which was used was a Skyscan 1172 (Orthopaedic engineering department, University of Edinburgh S/N=08F01110). The data was reconstructed using Skyscan reconstruction software and scanning was performed with a 360° rotation (resolution /pixel size = 2.9278 μ m, Source Voltage = 58 kV, Source Current = 171 μ A, Exposure = 1178 ms).

Metabolomics. MSCs were stimulated in 3D collagen gels (2mg/ml) at a density of 4×10^4 cells/ml of gel (2.5 ml) for 5 days or 2 days for the transient ion channel and PKC inhibition studies. Non-stimulated samples were used as controls. The metabolites were extracted using a 1:3:1 chloroform/methanol/water extraction buffer and placed on a shaking platform for 1 h at 4°C. The sample supernatant was transferred into 1.5 ml tubes and centrifuged for 3 min at 13,000g at 4°C. The samples were used for hydrophilic interaction liquid chromatography-mass spectrometry analysis (UltiMate 3000 RSLC, Thermo Fisher, with a 150 x 4.6 mm ZIC-pHILIC column running at 300 μ L/min and Orbitrap Exactive, Thermo Fisher, respectively). After Nanodrop (Thermo Fisher) measurement, total protein content was found identical in all samples, thus no further standardization was necessary. A standard pipeline, consisting of XCMS⁵⁴ (peak picking), MzMatch⁵⁵ (filtering and grouping), and IDEOM⁵⁶ (further filtering, post-processing and identification) was used to process the raw mass spectrometry data. Identified core metabolites were validated against a panel of unambiguous standards by mass and retention time. Further putative identifications were allotted by mass and predicted retention time⁵⁷. Means and standard errors of the mean were generated for every group of picked peaks and the resulting metabolomics data were uploaded to Ingenuity pathway analysis software for metabolite pathway analysis.

Statistics. Unless stated, one-way ANOVA and Kruskal Wallis with Dunn's post-test was used to compare significance in qPCR, in cell western and Von Kossa stain experiments. Two tailed, unpaired U-Tests (Mann Whitney) were performed where a direct comparison was assessed between only two population groups. A sample population of between 3 and 6 replicates were always used. All results are quoted as mean \pm standard deviation and the probability values have been quoted to an accuracy of 95%, 99% and 99.9% (* p < 0.05, ** p < 0.01 and *** p \leq 0.001 respectively). Supplementary Table 5 indicates samples numbers and replicates used in each figure presented.

Data Availability Statement.

The authors declare that all data supporting the findings of this study are available within the paper and its supplementary information. All raw data can be found at: <http://dx.doi.org/10.5525/gla.researchdata.327>

1. Giannoudis, P.V., Chris Arts, J.J., Schmidmaier, G. & Larsson, S. What should be the characteristics of the ideal bone graft substitute? *Injury* **42 Suppl 2**, S1-2 (2011).
2. Myeroff, C. & Archdeacon, M. Autogenous bone graft: donor sites and techniques. *J Bone Joint Surg Am* **93**, 2227-2236 (2011).
3. Dimitriou, R., Mataliotakis, G.I., Angoules, A.G., Kanakaris, N.K. & Giannoudis, P.V. Complications following autologous bone graft harvesting from the iliac crest and using the RIA: a systematic review. *Injury* **42 Suppl 2**, S3-15 (2011).
4. Garcia-Gareta, E., Coathup, M.J. & Blunn, G.W. Osteoinduction of bone grafting materials for bone repair and regeneration. *Bone* **81**, 112-121 (2015).
5. Dove, A. Drug screening--beyond the bottleneck. *Nat Biotechnol* **17**, 859-863 (1999).
6. Dalby, M.J. et al. The control of human mesenchymal cell differentiation using nanoscale symmetry and disorder. *Nat Mater* **6**, 997-1003 (2007).
7. Wen, J.H. et al. Interplay of matrix stiffness and protein tethering in stem cell differentiation. *Nat Mater* (2014).
8. Murphy, W.L., McDevitt, T.C. & Engler, A.J. Materials as stem cell regulators. *Nat Mater* **13**, 547-557 (2014).
9. Engler, A.J., Sweeney, H.L., Discher, D.E. & Schwarzbauer, J.E. Extracellular matrix elasticity directs stem cell differentiation. *J Musculoskelet Neuronal Interact* **7**, 335 (2007).
10. Curran, J.M. et al. Introducing dip pen nanolithography as a tool for controlling stem cell behaviour: unlocking the potential of the next generation of smart materials in regenerative medicine. *Lab Chip* **10**, 1662-1670 (2010).
11. Kloxin, A.M., Kasko, A.M., Salinas, C.N. & Anseth, K.S. Photodegradable hydrogels for dynamic tuning of physical and chemical properties. *Science* **324**, 59-63 (2009).
12. Benoit, D.S., Schwartz, M.P., Durney, A.R. & Anseth, K.S. Small functional groups for controlled differentiation of hydrogel-encapsulated human mesenchymal stem cells. *Nat Mater* **7**, 816-823 (2008).
13. Khetan, S. et al. Degradation-mediated cellular traction directs stem cell fate in covalently crosslinked three-dimensional hydrogels. *Nat Mater* **12**, 458-465 (2013).
14. Rauh, J., Milan, F., Gunther, K.P. & Stiehler, M. Bioreactor systems for bone tissue engineering. *Tissue engineering. Part B, Reviews* **17**, 263-280 (2011).
15. Epstein, N.E. Complications due to the use of BMP/INFUSE in spine surgery: The evidence continues to mount. *Surgical neurology international* **4**, S343-352 (2013).
16. Salter, E. et al. Bone tissue engineering bioreactors: a role in the clinic? *Tissue engineering* **18**, 62-75 (2012).
17. Pemberton, G.D. et al. Nanoscale stimulation of osteoblastogenesis from mesenchymal stem cells: nanotopography and nanokicking. *Nanomedicine (Lond)* **10**, 547-560 (2015).
18. Nikukar, H. et al. Osteogenesis of mesenchymal stem cells by nanoscale mechanotransduction. *ACS Nano* **7**, 2758-2767 (2013).
19. McBeath, R., Pirone, D.M., Nelson, C.M., Bhadriraju, K. & Chen, C.S. Cell shape, cytoskeletal tension, and RhoA regulate stem cell lineage commitment. *Dev Cell* **6**, 483-495 (2004).

20. Kilian, K.A., Bugarija, B., Lahn, B.T. & Mrksich, M. Geometric cues for directing the differentiation of mesenchymal stem cells. *Proc Natl Acad Sci U S A* **107**, 4872-4877 (2010).
21. Abbott, B.P. et al. Observation of Gravitational Waves from a Binary Black Hole Merger. *Phys Rev Lett* **116**, 061102 (2016).
22. Hakansson, B., Brandt, A., Carlsson, P. & Tjellstrom, A. Resonance frequencies of the human skull in vivo. *The Journal of the Acoustical Society of America* **95**, 1474-1481 (1994).
23. Dalby, M.J., Gadegaard, N. & Oreffo, R.O. Harnessing nanotopography and integrin-matrix interactions to influence stem cell fate. *Nature materials* **13**, 558-569 (2014).
24. McNamara, L.E. et al. Skeletal stem cell physiology on functionally distinct titania nanotopographies. *Biomaterials* **32**, 7403-7410 (2011).
25. Yang, J. et al. Nanotopographical Induction of Osteogenesis through Adhesion, Bone Morphogenic Protein Cosignaling, and Regulation of MicroRNAs. *ACS Nano* **8**, 9941-9953 (2014).
26. Engler, A.J., Sen, S., Sweeney, H.L. & Discher, D.E. Matrix elasticity directs stem cell lineage specification. *Cell* **126**, 677-689 (2006).
27. Masuyama, R. et al. TRPV4-mediated calcium influx regulates terminal differentiation of osteoclasts. *Cell metabolism* **8**, 257-265 (2008).
28. Coste, B. et al. Piezo proteins are pore-forming subunits of mechanically activated channels. *Nature* **483**, 176-181 (2012).
29. Kim, S.E., Coste, B., Chadha, A., Cook, B. & Patapoutian, A. The role of Drosophila Piezo in mechanical nociception. *Nature* **483**, 209-212 (2012).
30. Kuipers, A.J., Middelbeek, J. & van Leeuwen, F.N. Mechanoregulation of cytoskeletal dynamics by TRP channels. *European journal of cell biology* **91**, 834-846 (2012).
31. Bando, Y., Hirano, T. & Tagawa, Y. Dysfunction of KCNK potassium channels impairs neuronal migration in the developing mouse cerebral cortex. *Cerebral cortex* **24**, 1017-1029 (2014).
32. Lee, W. et al. Synergy between Piezo1 and Piezo2 channels confers high-strain mechanosensitivity to articular cartilage. *P Natl Acad Sci USA* **111**, E5114-E5122 (2014).
33. Zhang, W., Yan, Z., Jan, L.Y. & Jan, Y.N. Sound response mediated by the TRP channels NOMPC, NANCHUNG, and INACTIVE in chordotonal organs of Drosophila larvae. *Proc Natl Acad Sci U S A* **110**, 13612-13617 (2013).
34. Maksimovic, S. et al. Epidermal Merkel cells are mechanosensory cells that tune mammalian touch receptors. *Nature* **509**, 617-621 (2014).
35. Lieben, L. & Carmeliet, G. The Involvement of TRP Channels in Bone Homeostasis. *Front Endocrinol (Lausanne)* **3**, 99 (2012).
36. Idris, A.I., Landao-Bassonga, E. & Ralston, S.H. The TRPV1 ion channel antagonist capsaizepine inhibits osteoclast and osteoblast differentiation in vitro and ovariectomy induced bone loss in vivo. *Bone* **46**, 1089-1099 (2010).
37. Clapham, D.E. TRP channels as cellular sensors. *Nature* **426**, 517-524 (2003).
38. Bae, C., Sachs, F. & Gottlieb, P.A. The mechanosensitive ion channel Piezo1 is inhibited by the peptide GsMTx4. *Biochemistry* **50**, 6295-6300 (2011).
39. Chen, J. et al. Selective blockade of TRPA1 channel attenuates pathological pain without altering noxious cold sensation or body temperature regulation. *Pain* **152**, 1165-1172 (2011).
40. Lee, L.C. et al. Nanotopography controls cell cycle changes involved with skeletal stem cell self-renewal and multipotency. *Biomaterials* **116**, 10-20 (2017).

41. Ge, C. et al. Reciprocal Control of Osteogenic and Adipogenic Differentiation by ERK/MAP Kinase Phosphorylation of Runx2 and PPARgamma Transcription Factors. *J Cell Physiol* **231**, 587-596 (2016).
42. Cheema, U., Chuo, C.-P., Sarathchandra, P., Nazhat, S.N. & Brown, R.A. Engineering Functional Collagen Scaffolds: Cyclical loading Increases Material Strength and Fibril Aggregation. *Advanced Functional Materials* **17**, 2426-2431 (2007).
43. Discher, D.E., Mooney, D.J. & Zandstra, P.W. Growth factors, matrices, and forces combine and control stem cells. *Science* **324**, 1673-1677 (2009).
44. Swift, J. et al. Nuclear lamin-A scales with tissue stiffness and enhances matrix-directed differentiation. *Science* **341**, 1240104 (2013).
45. Huebsch, N. et al. Harnessing traction-mediated manipulation of the cell/matrix interface to control stem-cell fate. *Nat Mater* **9**, 518-526 (2010).
46. Lai, V.K., Lake, S.P., Frey, C.R., Tranquillo, R.T. & Barocas, V.H. Mechanical behavior of collagen-fibrin co-gels reflects transition from series to parallel interactions with increasing collagen content. *Journal of biomechanical engineering* **134**, 011004 (2012).
47. Gentleman, E. et al. Comparative materials differences revealed in engineered bone as a function of cell-specific differentiation. *Nat Mater* (2009).
48. Vandorpe, D.H. & Morris, C.E. Stretch activation of the *Aplysia* S-channel. *J Membr Biol* **127**, 205-214 (1992).
49. Stein, G.S. & Lian, J.B. Molecular mechanisms mediating proliferation/differentiation interrelationships during progressive development of the osteoblast phenotype. *Endocr Rev* **14**, 424-442 (1993).
50. Liu, Y. et al. Hydrogen sulfide maintains mesenchymal stem cell function and bone homeostasis via regulation of Ca(2+) channel sulfhydration. *Cell Stem Cell* **15**, 66-78 (2014).
51. Gaur, T. et al. Canonical WNT signaling promotes osteogenesis by directly stimulating Runx2 gene expression. *J Biol Chem* **280**, 33132-33140 (2005).
52. Tsimbouri, P.M. et al. Using nanotopography and metabolomics to identify biochemical effectors of multipotency. *ACS Nano* **6**, 10239-10249 (2012).
53. Agosti, J.K., Chandler, L.A., Anderton, C.M. & Clark, R.M. Serial sharp debridement and formulated collagen gel to treat pressure ulcers in elderly long-term care patients: a case study. *Ostomy Wound Manage* **59**, 43-49 (2013).
54. Smith, C.A., Want, E.J., O'Maille, G., Abagyan, R. & Siuzdak, G. XCMS: processing mass spectrometry data for metabolite profiling using nonlinear peak alignment, matching, and identification. *Anal Chem* **78**, 779-787 (2006).
55. Scheltema, R.A., Jankevics, A., Jansen, R.C., Swertz, M.A. & Breitling, R. PeakML/mzMatch: a file format, Java library, R library, and tool-chain for mass spectrometry data analysis. *Anal Chem* **83**, 2786-2793 (2011).
56. Creek, D.J., Jankenevics, A., Burgess, K.V., Breitling, R. & Barrett, M.P. IDEOM: An excel interface for analysis of LC-MS based metabolomics data. *BMC Bioinformatics In Press* (2012).
57. Creek, D.J. et al. Toward global metabolomics analysis with hydrophilic interaction liquid chromatography-mass spectrometry: improved metabolite identification by retention time prediction. *Anal Chem* **83**, 8703-8710 (2011).

Figure 1. Development of the nanovibrational bioreactor. (a) The nanovibrational bioreactor consists of a piezo-driven vibrational plate set on top of a heavy base block

to direct vibration upwards. Culture ware is magnetically attached to the top plate and vibrated at the nanoscale according to the input voltage signal. (b) ANSYS finite element modelling of the bioreactor top plate and a magnetic culture plate. Harmonic response analysis shows the amplitude response when both are vibrated (30 nm, 1000 Hz), showing a high level of consistency is to be expected across the cell growth surface. (c) ANSYS harmonic response modelling of the growth surface of a 6-well plate in the range of 0 to 10,000 Hz (30 nm amplitude). Response of the growth surface follows the input vibration reliably until reaching 3000 Hz (insert shows 1000 Hz). Above this frequency, resonances cause large amplification and deformations at the growth surface shown by the minimum and maximum amplitudes taken from the modelled surface. (d) Laser interferometric testing of the bioreactor top plate and growth substrate. Mirrored pieces of silicon are bonded to the measurement point on the top plate or placed atop the growth surface to reflect a laser beam. This allows the vibration amplitude to be measured to sub-nm resolution. (e) Interferometric calibration of the bioreactor for five frequencies. Vibration amplitude is linearly dependant on the input voltage (peak to peak) of the bioreactor (actuators wired in series). Divergence occurs at 4000 Hz due to resonant amplification, as predicted by the Ansys model (shown in (c)). (f) MSCs were stimulated (1000Hz) on the vibrational bioreactor for 7 days and their mRNA levels then measured by qPCR. Osterix mRNA levels were significantly up-regulated compared to non-vibrated controls. Donors (d)=3, replicates per donor (r)= 4, technical replicates per replicate (t) = 2; results = mean \pm SD, stats by Mann Whitney U-test where ***p<0.001. (g) In-cell western analysis of MSCs after 2 and 3 weeks of nanovibrational stimulation compared to control MSCs and osteoblasts cultured for similar times. Results show that both nanovibrated cells and osteoblasts had an enhanced osteoblast phenotype compared to untreated MSCs by measurement of ALP and OPN. D=1, r=3, results = mean \pm SD, stats for treatment compared to control by ANOVA and Tukey test where *p<0.05 and ***p<0.001 (dots represent individual data points). (h) In-cell western of pERK1/2 / total ERK1/2 in cells released from synchronisation (1 hour seeding in 10% serum and serum withdrawal for 24 hours). After reintroduction of 10% serum and commencement of nanovibrational stimulation (1000 Hz) (with control cells receiving no stimulation) for 23 hours, inhibitors of channels Piezo1 (GsMTx4) and TRPV1

(QX314) were added for 1 hour. pERK 1/2 levels were reduced only in MSCs undergoing nanovibrational stimulation when either channel was blocked. $D=3$, $r=4$, results = mean \pm SD, stats by ANOVA and Kruskal Wallis test where $**p<0.01$ and $***p<0.001$.

Figure 2. Characterization of 3D-collagen gel culture on the vibrational bioreactor.

(a) Rheological assessment of the collagen gel without MSCs. Comparison of complex shear moduli values show that a soft gel has been formed rather than a liquid state (i.e. $G'>G''$). Conversion yields an elastic modulus equalling ~ 108 Pa. (b) Similar results were obtained for collagen gel that contains 100,000 MSCs. These samples yield an elastic modulus equalling ~ 74 Pa. (c) Stress-strain curve for the collagen gel constructs. For low values of shear deformation or shear stress, the material responds linearly. (d) ANSYS deformation modelling of a modelled polystyrene well, replicating one well of a 6-well plate whilst being vibrated (1000 Hz, 20 nm). The polystyrene shows consistent replication of vibration amplitude with minor edge reduction of less than 10%. (e) Mapping deformation of a vibrated gel (1000 Hz, 20 nm) within a modelled polystyrene well. The average vibration amplitude was consistent with the driving vibration when modelled as incompressible although on average slightly increased amplitudes were seen at the edge where a meniscus was present, replicating interferometric results. (f) Mapping shear stress during vibration at 1000 Hz, 20 nm amplitude. When compared with experimental values in (c), low levels of shear stress indicate that the gel should respond as a linear elastic material when vibrated under these conditions (1000 Hz, 20 nm). (g) Picture of the apparatus, including 2.5 ml samples of collagen gel, whilst being tested using laser interferometry. Silicon fragments of 50 μ m thickness were placed on the surface of the gel to measure transmission of the underlying vibration amplitude. Measurements were taken both at the centre of each well and at the edge where a meniscus was present. (h) Interferometric calibration of the gel for five vibration frequencies. Vibration amplitude is linearly dependant on the input voltage (peak to peak) of the bioreactor. (i) Graph showing the nanometre displacement measurements in the range of 500 to 5000 Hz with a set voltage of 12 Vpk-pk. Data is shown for the centre and outer edge of each well whilst being either empty, filled with 2.5ml collagen gel, or with 2.5ml collagen gel seeded with $\sim 100,000$ MSCs. Resonant peaks can be

seen at frequencies of 2500, 3500 and 5000 Hz with gel vibration consistently following the underlying substrate below 2000 Hz. The inset shows the specific variances, including increased edge amplitude (dashed lines), at the experimental frequency of 1000 Hz, replicating the modelled results in (d) and (e). Interferometric results show mean values \pm SD (n=3).

Figure 3. Confirmation of bone mineralisation in 3D through nanovibrational stimulation. (a) Time course qPCR analysis of BMP2, RUNX2, ALP, OPN, OCN and collagen I transcripts, showing significantly higher expression in 3D nanovibrated MSCs compared to control 3D cultures at the same time point. Donors (d)=1, replicates per donor (r)= 6, technical replicates per replicate (t) = 2; results = mean \pm SD, stats by Mann Whitney U-test where *p<0.05, **p<0.01 and ***p<0.001. Values are log scale. (b) Von Kossa staining and quantification. Staining performed after 6 weeks of nanovibrations at 1000 Hz in 3D. Gels shown (on left) were removed from a 6-well plate before processing. The intensity of von Kossa staining was measured against unstimulated controls and osteospecific media (OSM). A significantly increased level of staining was observed for the nanostimulated samples relative to the unstimulated controls after 4 weeks (d=3 (d=1 for OSM), r=4), and for nanostimulated samples and OSM-treated cells after 6 weeks (d=1, r=5). Results are mean \pm SD where *p<0.05, **p<0.01 and ***p<0.001 by ANOVA and Kruskal Wallis test (individual data points are shown as dots). (c) Raman spectra for bovine cortical compact bone, this profile was used as a reference standard to characterise the Raman scattering (fingerprint identification region 500 cm⁻¹ – 1500 cm⁻¹) pattern of bone. Predominant peaks observed at ~ 960 cm⁻¹ (arrow) and ~ 1072 cm⁻¹ (arrowhead) correspond to PO₄³⁻ v₁ and CO₃²⁻ bond stretching, respectively. (d) For the control sample, MSCs were cultured in a collagen gel for 46 days. Raman spectroscopy showed no phosphate peak present. (f) MSCs nanovibrated for 46 days at 1000 Hz in a collagen matrix. Raman spectroscopy showed peaks matching the main peaks of the cortical bone sample. D=1, r=3, Scale bar = 50 μ m. (e) MSCs cultured for 35 days in a collagen matrix and imaged by μ CT showing no bone deposits. (g) MSCs nanovibrated at 1000 Hz for 35 days in a collagen matrix and imaged by μ CT showing mineral deposits (arrow). Scale bar = 200 μ m. MSCs

were seeded at 40,000 cells/ml; for the μ CT analysis, a higher cell concentration, 300,000 cells/ml, was used.

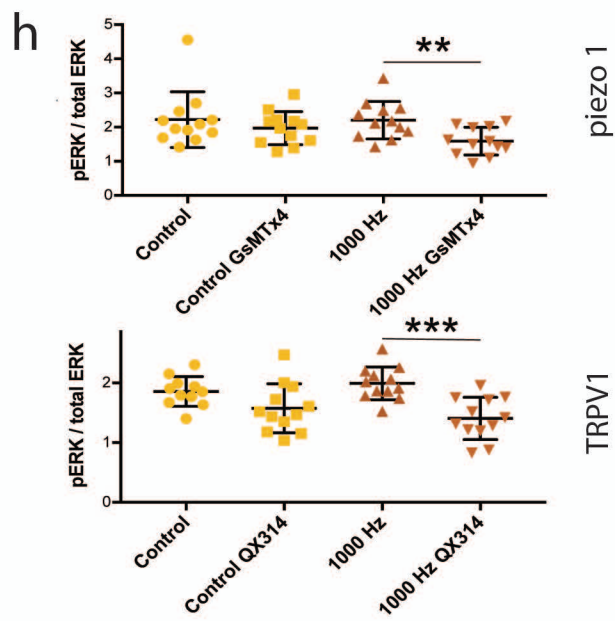
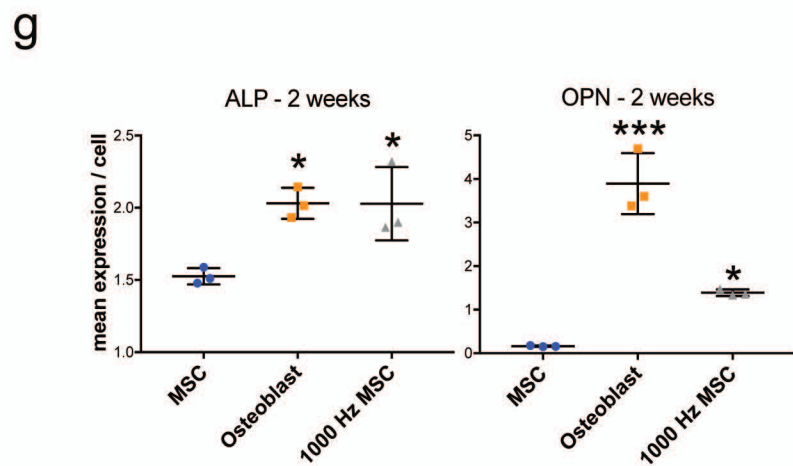
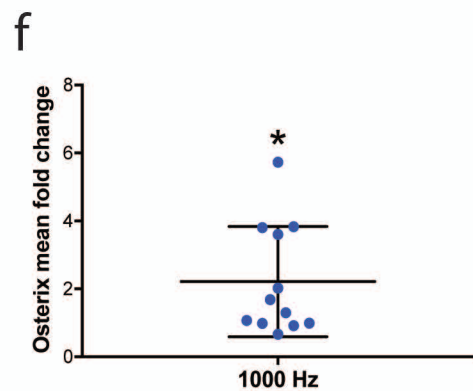
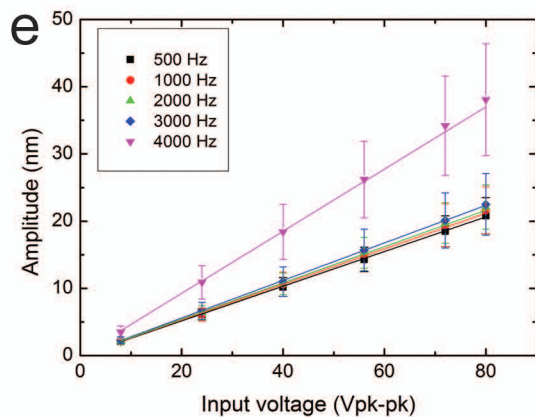
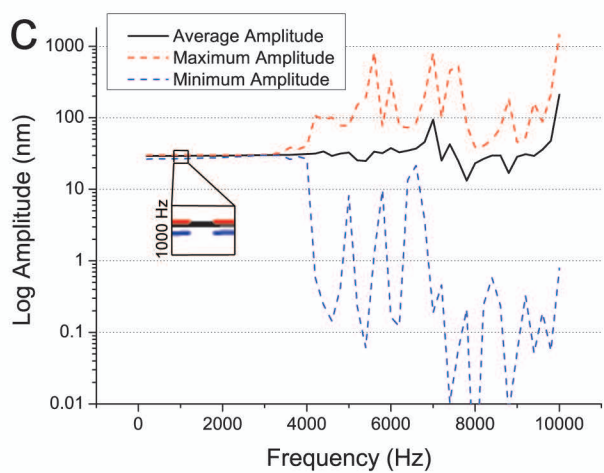
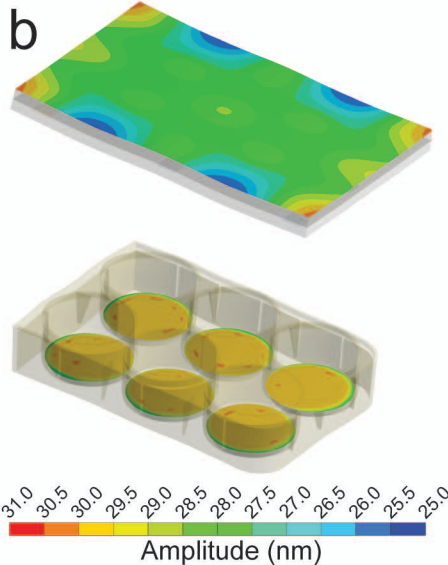
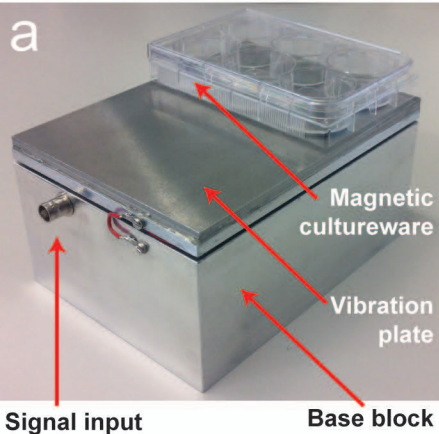
Figure 4. Testing for channel and phenotype sensitivity to cytoskeletal tension. (a) Temporal qPCR data for Piezo 1, Piezo2, TRPV1 and KCNK2 transcripts in MSCs after 3, 5, 7, 14 and 21 days of 3D nanovibrational stimulation compared to control cultures. A biphasic trend of high to low expression, recovery, and high to low expression was noted with significant downregulation of all the receptor transcripts seen at day 21. Donors (d)=1, replicates per donor (r)= 6 (3 for days 3 and 5), technical replicates per replicate (t) = 2; results = mean \pm SEM, stats by Mann Whitney U-test where * p <0.05 and *** p <0.001. Values are log scale. (b-e) qPCR analysis for Piezo 1 (b), Piezo 2 (c), KCNK2 (d) and TRPV1 (e) expression in MSCs after 5 days of nanovibrational stimulation or of OSM stimulation, compared to control cultures, with addition of the ROCK inhibitor (Y27632) or the myosin II inhibitor (blebbistatin). Cytoskeletal tension dependencies were noted for Piezo 2 (c) and TRPV1 (e), with increased significance noted when osteogenesis was stimulated by nanovibration compared to stimulation by OSM. D=3, r=4, t=2; results = mean \pm SEM, stats by ANOVA and Kruskal Wallis test where * p <0.05 and ** p <0.01. Values are log scale. (f-h) qPCR analysis of BMPR1a (f), RUNX2 (g) and ALP (h) expression, in MSCs after 5 days of nanovibrational stimulation (1000Hz) compared to control cultures, with addition of Y27632 or blebbistatin. Cytoskeletal tension dependencies were noted for BMPR1a (f) at this time point. D=2, r=3, t=2; results = mean \pm SEM, stats by ANOVA and Tukey test where * p <0.05 and *** p <0.001. Values are log scale.

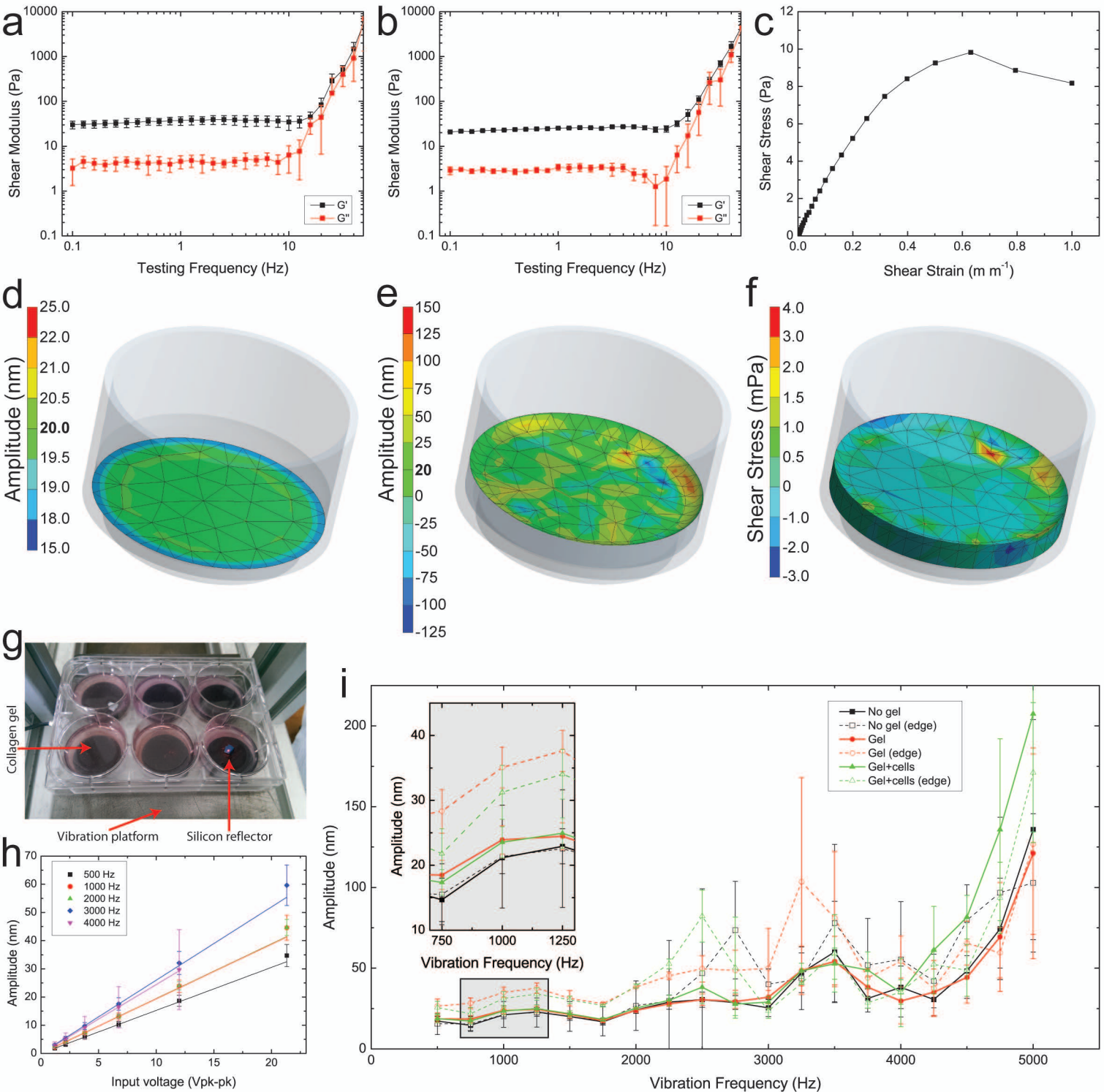
Figure 5. Testing for TRPV involvement in nanovibration-stimulated osteogenic pathways. (a) Western-blot densitometry data for pFAK/total FAK, pMyosin/total myosin, pERK/total ERK, pSMAD1/5/8 / total SMAD 1/5/8 and active β -catenin / lane loading control with/without PKC inhibition (inhibition denoted by "I") after 5 days of nanovibrational (1000Hz) stimulation. Active β -catenin was significantly reduced following PKC inhibition. Data is mean relative to unstimulated control for donors (d)

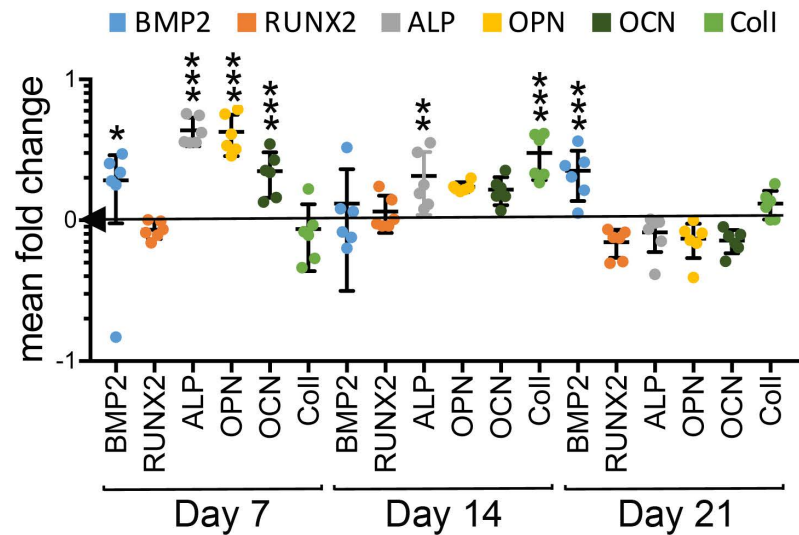
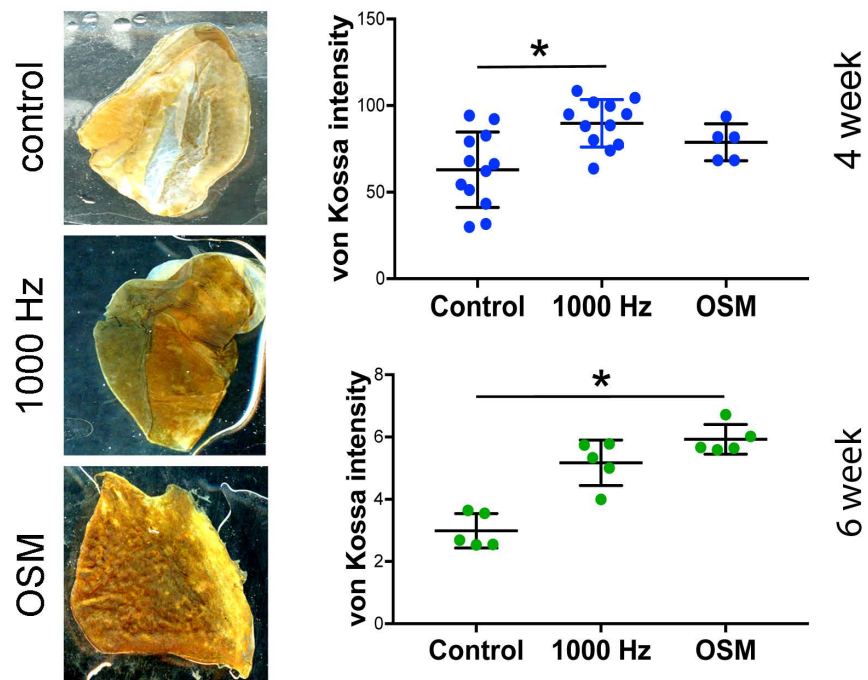
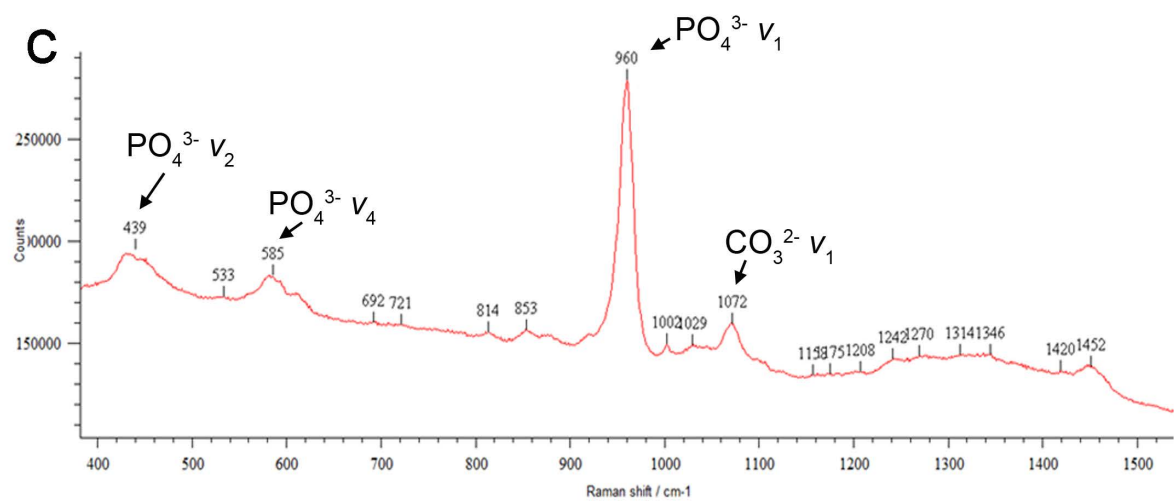
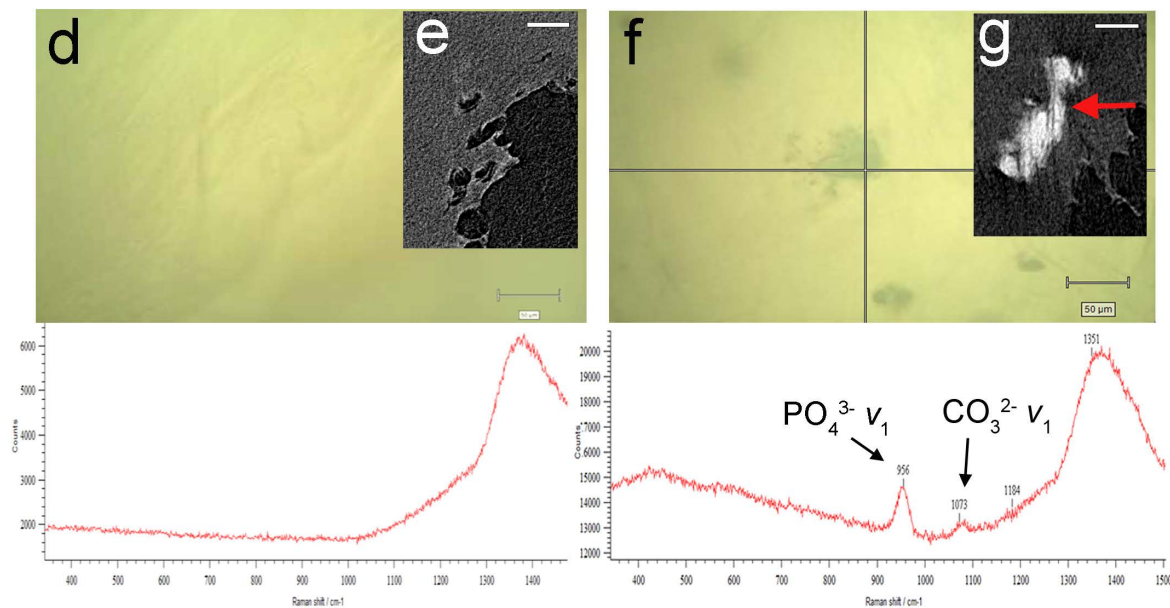
= 3, replicated per donor (r) (pooled) = 4, results = mean \pm SD, stats by Tukey test where * p <0.05. (b) Western-blot densitometry for total ERK/lane loading control and total β -catenin/lane loading control with/without PKC (1000 Hz-PKC) and TRPV (1000 Hz-TRPV) inhibition. Total β -catenin was significantly reduced with PKC and TRPV inhibition. Data is mean relative to unstimulated control for $d = 3$, r (pooled) = 4, results = mean \pm SD, stats by Tukey test where * p <0.05.

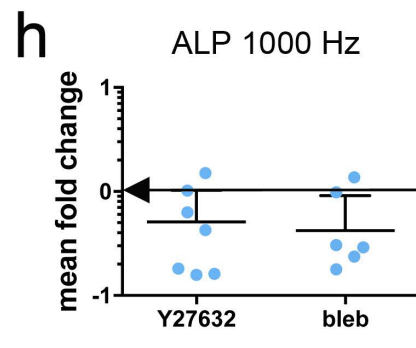
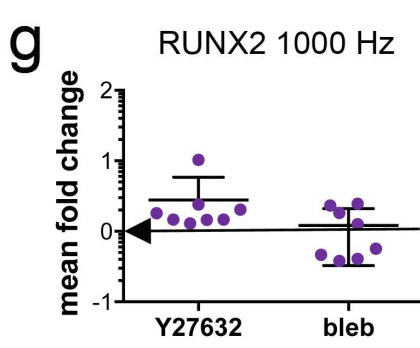
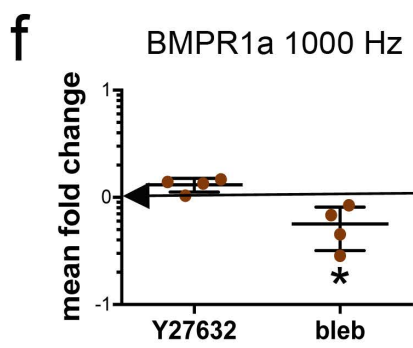
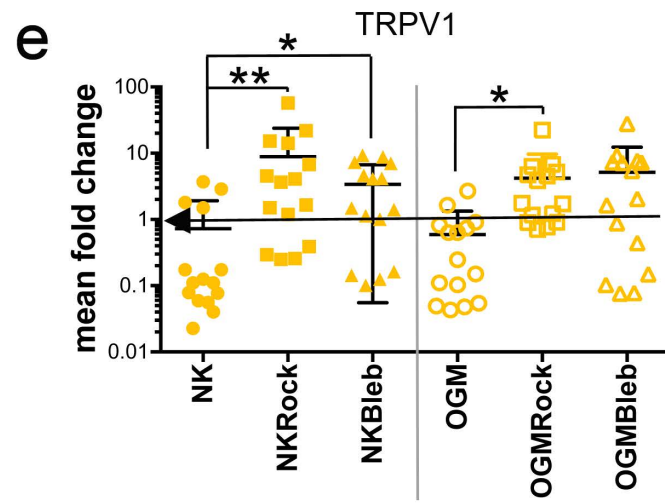
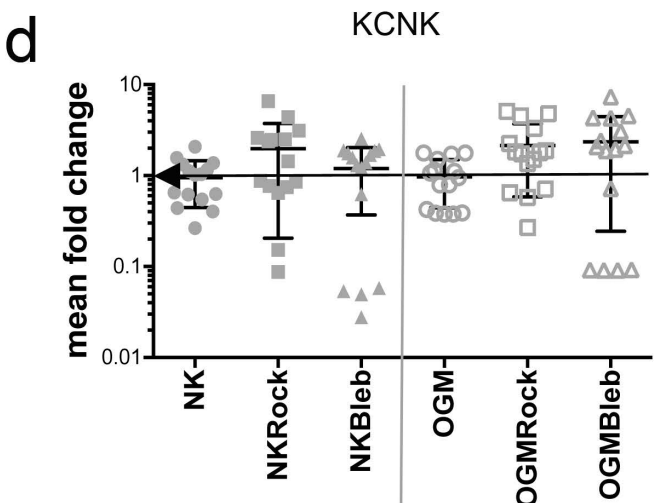
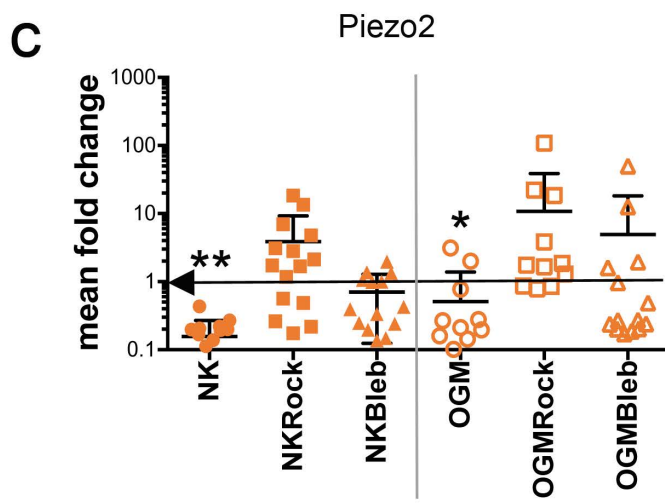
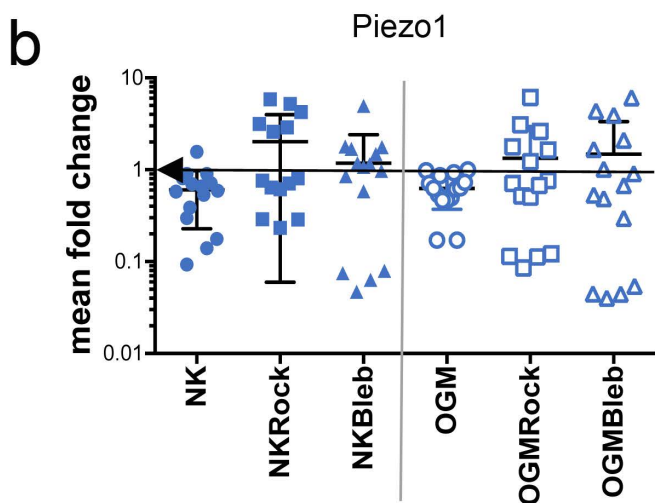
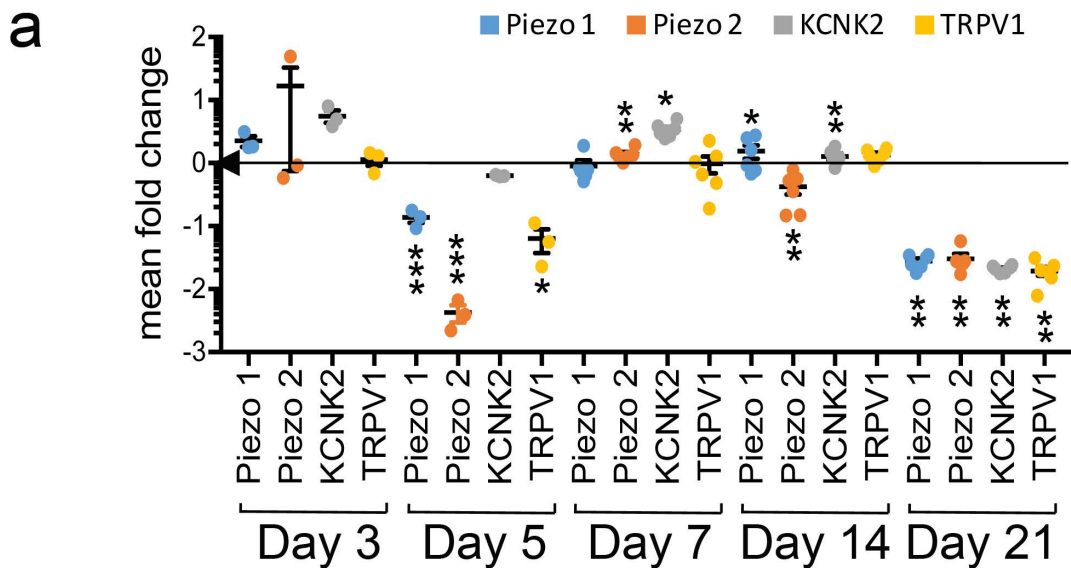
Figure 6. Testing for TRPV and wnt involvement in nanovibration-stimulated osteogenic stimulation using metabolomics. (a-c) Metabolic networks, generated in IPA by uploading of metabolite data and use of predictive biochemical interactions, that link metabolite changes to signalling hubs, such as ERK and the canonical Wnt signalling pathway. (a) The network for 1000 Hz-stimulated cells, demonstrating the mainly predicted biochemical up-regulation of these pathways. (b) The network for 1000 Hz-PKC inhibition, showing a trend towards predicted down-regulation. (c) The network for 1000 Hz-TRPV down-regulation, showing broadly predicted down-regulations. See key for pathway information, data is mean relative to unstimulated control for $d=3$, $r=4$. (d) Schematic showing possible osteogenesis inducing mechanisms that were tested, with the TRP- β -catenin pathways highlighted as a pathway that we have proposed as being central to MSC nanovibrational osteogenesis.

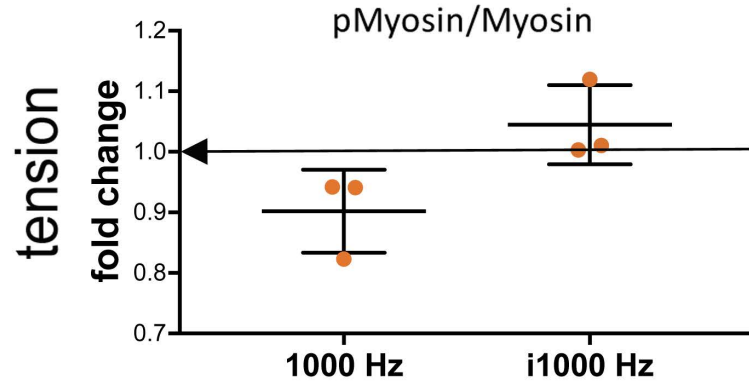
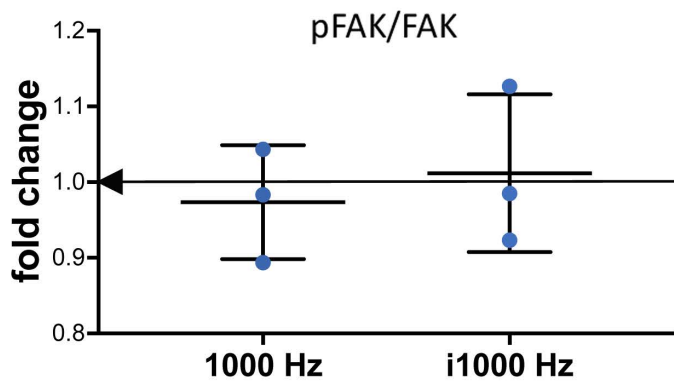
Figure 7. Testing for TRPV involvement in nanovibration stimulated osteogenesis. QPCR data for the osteospecific genes BMPR1a and BMP2 (very early stage), RUNX2 (early stage) and ALP and osteonectin (mid-stage osteogenesis) after 5 days of stimulation. For 1000 Hz PKC and 1000 Hz TRPV, data is relative to 1000 Hz vs non-stimulated control. Cells were inhibited for the final 24 hours of culture. Data shows loss of osteoblastic phenotype progression for PKC inhibition (BMP2) and TRPV inhibition (BMP2, RUNX2, ALP and osteonectin (OSN)). Data is mean \pm SD for donors (d) = 3, replicated per donor (r) = 4, technical replicates (t) = 2. Data was shown to be normally distributed, stats by Tukey test where * p <0.05 and ** p <0.01.



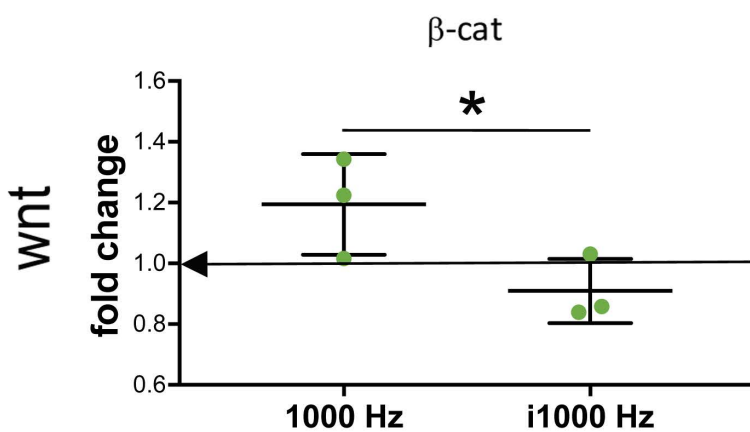
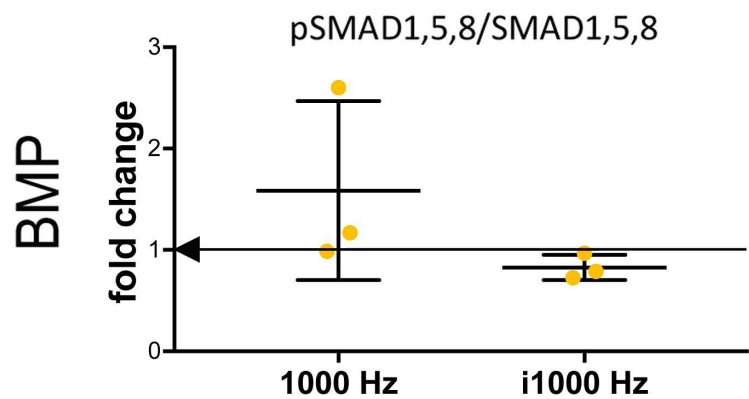
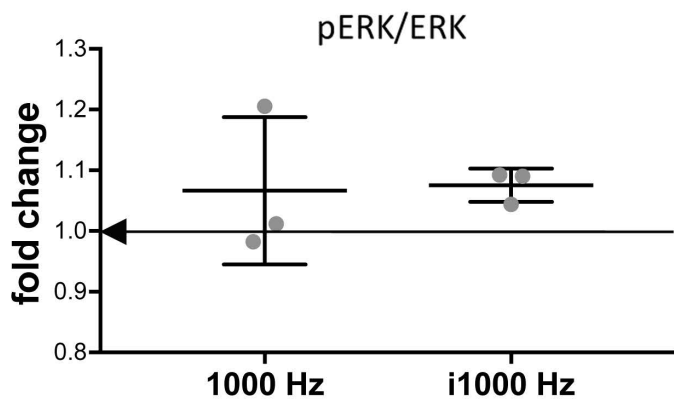
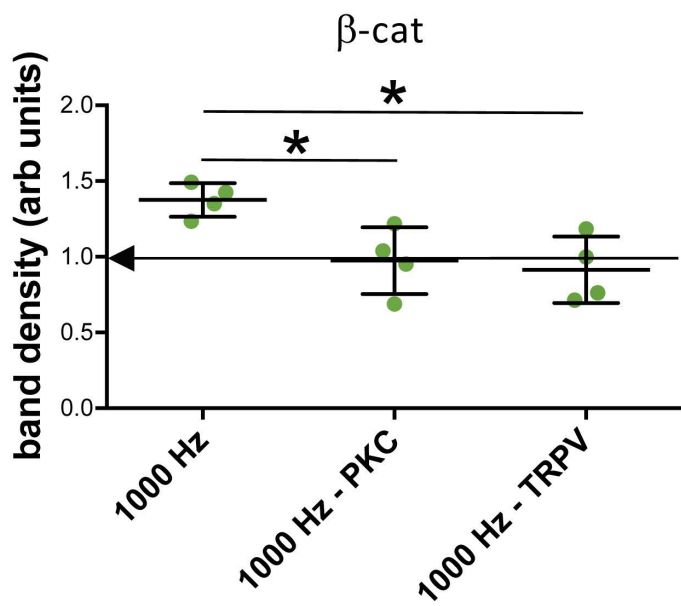
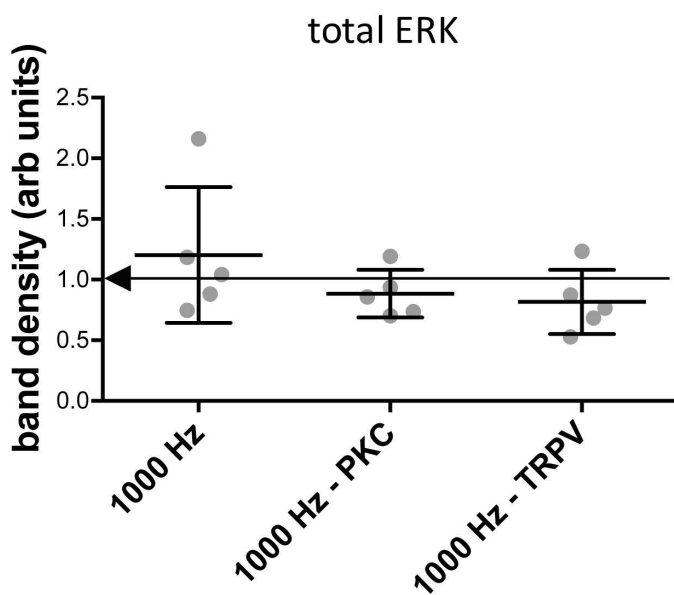


a**b****c****d**



a
adhesion

ERK

**b**

fold change to 1000 Hz



1000 Hz - PKC

]BMPR1a

1000 Hz - TRPV

1000 Hz - PKC

]BMP2

1000 Hz - TRPV

1000 Hz - PKC

]RUNX2

1000 Hz - TRPV

1000 Hz - PKC

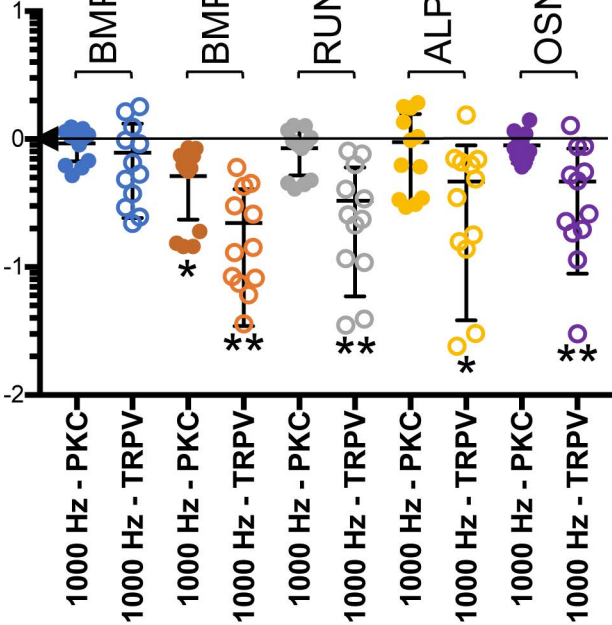
]ALP

1000 Hz - TRPV

1000 Hz - PKC

]OSN

1000 Hz - TRPV



Supplementary information for:

Stimulation of 3D osteogenesis by mesenchymal stem cells via a nanovibrational bioreactor.

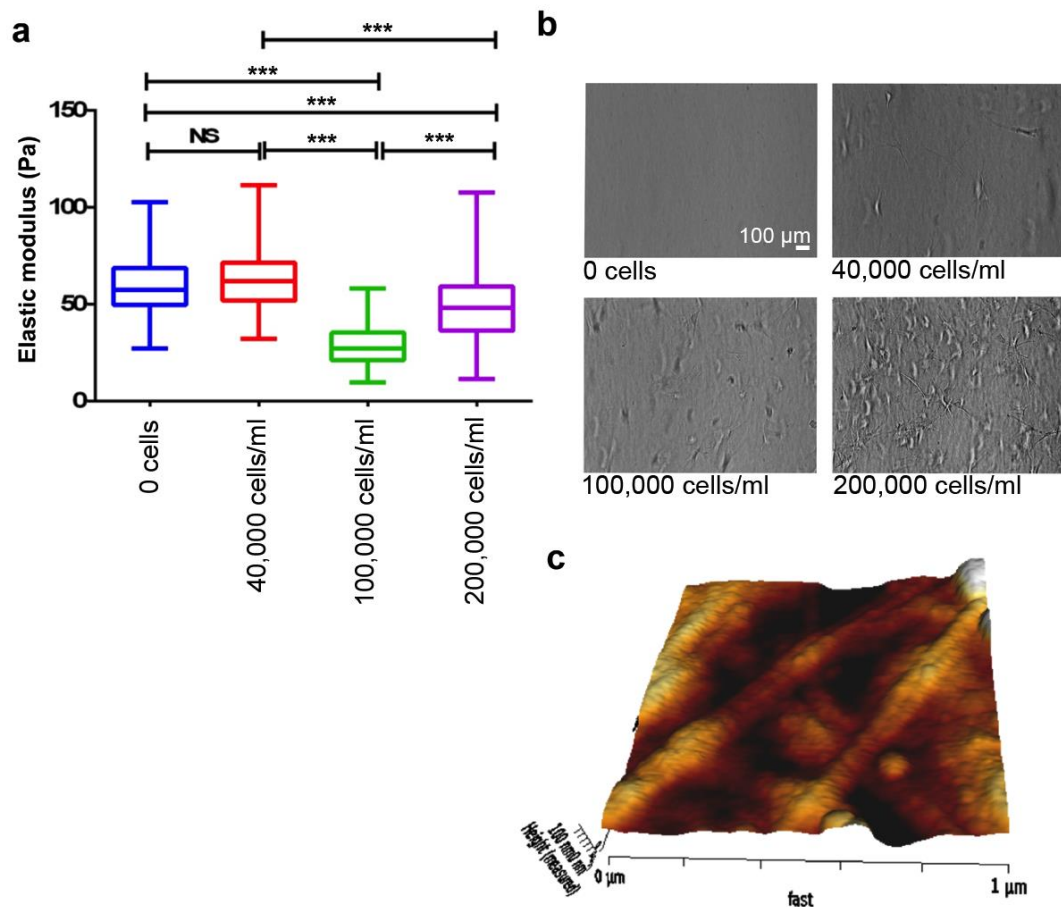
P. Monica Tsimbouri, Peter G. Childs, Gabriel D. Pemberton, Jingli Yang, Vineetha Jayawarna, Wich Orapiriyakul, Karl Burgess, Cristina Gonzalez-Garcia, Gavin Blackburn, Dilip Thomas, Catalina V. Giraldo, Manus J.P. Biggs, Adam S.G. Curtis, Manuel Salmeron-Sanchez, Stuart Reid, Matthew J. Dalby

Table of contents.

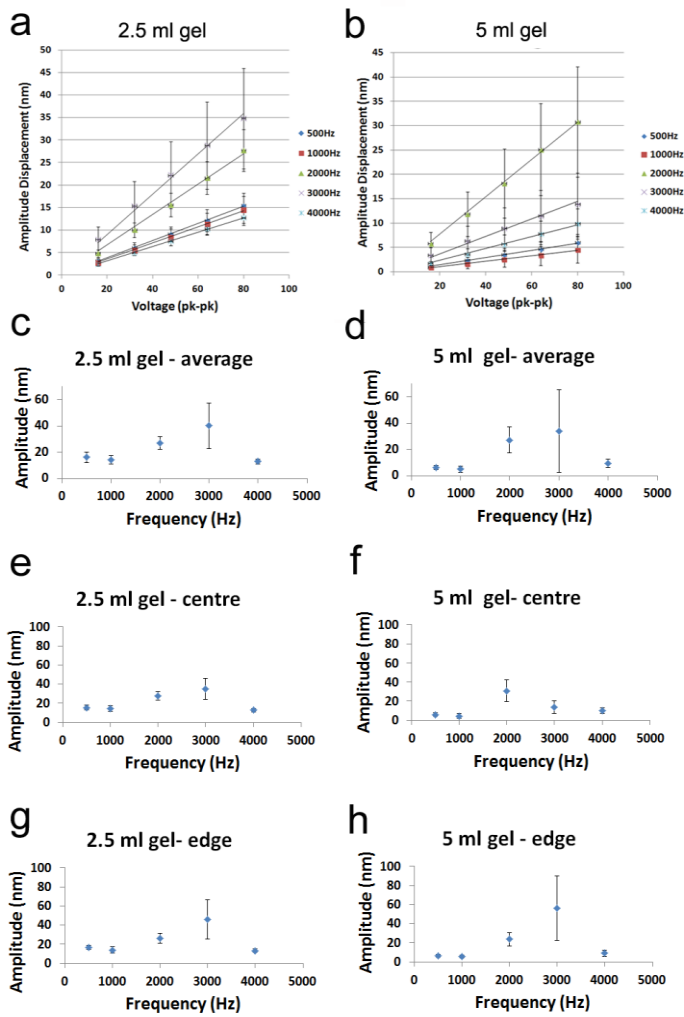
Item	Title	Page
<i>S</i> Table 1	<i>Material properties of the collagen gels, with and without MG63 cells.</i>	3
<i>S</i> Fig 1	<i>AFM stiffness measurements with increased cell loading.</i>	3
<i>S</i> Fig 2	<i>Comparison of 2.5 mL and 5.0 mL collagen gel fill on the nanovibration effect.</i>	4
<i>S</i> Fig 3	<i>Viability and metabolic activity of MSCs seeded into collagen gels with/without nanovibrational stimulation.</i>	5
<i>S</i> Fig 4	<i>Osteogenic assessment of nanovibration on bone protein expression.</i>	6
<i>S</i> Fig 5	<i>Further Raman Spectra.</i>	6
<i>S</i> Table 2	<i>Quantitative results of Raman scattering.</i>	7
<i>S</i> Fig 6	<i>Analysis of osteoblast genes at 14 days of culture after inhibition of intracellular tension.</i>	7
<i>S</i> Fig 7	<i>Metabolomics links to canonical signalling pathways.</i>	8
<i>S</i> Fig 8	<i>Heatmap of lipid metabolism.</i>	9
<i>S</i> Fig 9	<i>Heatmap of carbohydrate metabolism.</i>	10
<i>S</i> Fig 10	<i>Western blot analysis for 3D cultures.</i>	11
<i>S</i> Fig 11	<i>Western blots corresponding to Figure 5b.</i>	12
<i>S</i> Fig 12	<i>Metabolomics links to wnt signalling for nanovibrationally stimulated MSCs after 5 days of culture.</i>	13
<i>S</i> Fig 13	<i>Metabolomics links to wnt signalling for NS-PKC stimulated MSCs after 5 days of culture.</i>	14
<i>S</i> Fig 14	<i>Metabolomics links to wnt signalling for NS-TRPV stimulated MSCs after 5 days of culture.</i>	15
<i>S</i> Table 3	<i>RT-PCR Reverse transcription thermal programme.</i>	16
<i>S</i> Table 4	<i>Primers for genes used to perform qPCR.</i>	17
<i>S</i> Table 5	<i>Information regarding biological experiment replicate numbers linked to the figures.</i>	18
<i>S</i> References	<i>Supplementary references.</i>	18

Supplementary table 1. Material properties of the collagen gels, with and without MG63 cells. Values for shear moduli were taken from rheological measurement and used to calculate elastic and bulk moduli. Gels were seeded with 40,000 MG63 osteoblasts / ml). Results are mean \pm SD, N=3. Note MG63 cells were used for interferometry as a model cell to prevent using primary human cells with equipment in a non-class II environment. Further note that modulus falls sharply when >100,000 cell/ml were seeded.

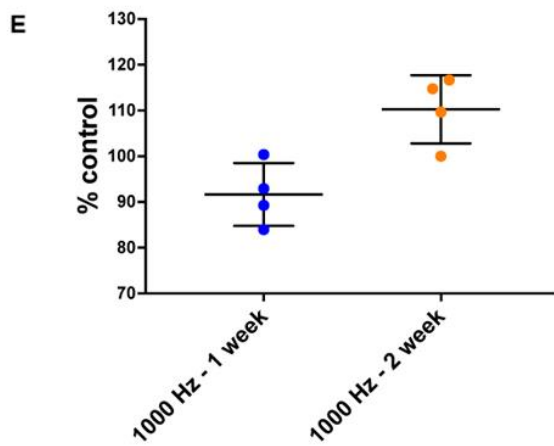
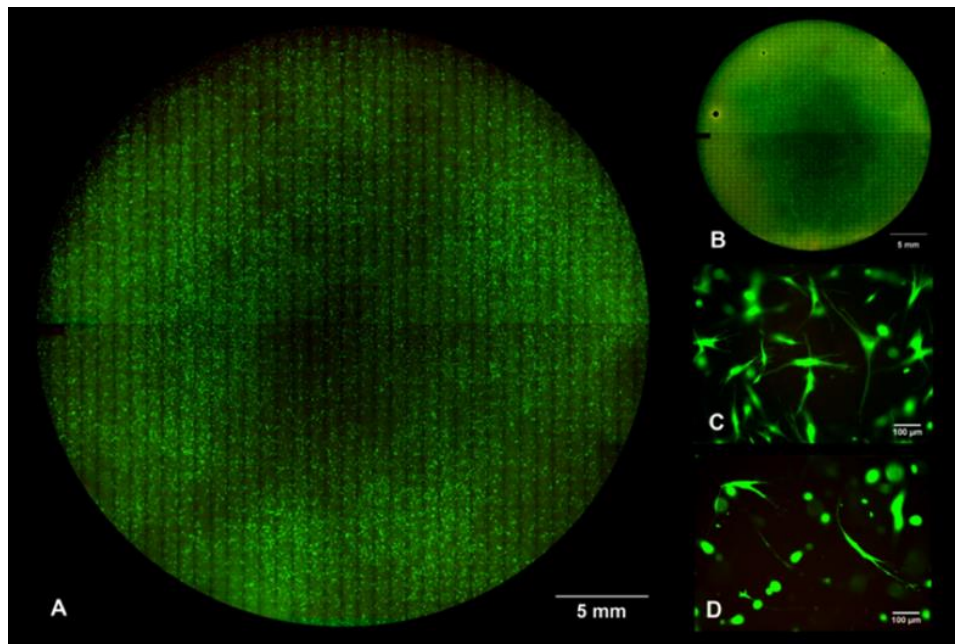
	Shear Moduli, G (Pa)	Elastic Moduli, E (Pa)	Bulk Moduli, K (MPa)	Poisson Ratio, ν
Collagen	36 \pm 7.4	108 \pm 22.2	1800 \pm 370	0.5
Collagen/cells	24.5 \pm 2.3	73.5 \pm 6.3	1225 \pm 105	0.5



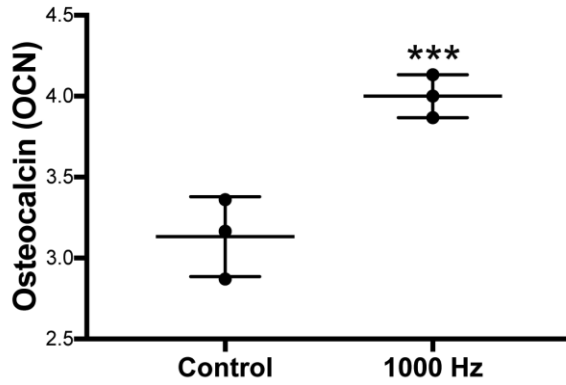
Supplementary Figure 1. AFM stiffness measurements with increased cell loading. Values for elastic moduli were taken using AFM in tapping mode. Gels were seeded with 40,000 MG63 osteoblasts / ml in 2.5 ml gels. (A) data showed that stiffness was reduced if >40,000 cells were used (n=3, results show median with second and third quartiles (box) and upper and lower quartiles (whiskers), stats by ANOVA with Tukey test where $*=p<0.05$, $**=p<0.01$, and $***=p<0.001$). (B) Increase in cell density in the gels could be seen using phase microscopy and (C) AFM revealed cells within collagen fibrils (gel with 200,000 cells/ml shown).



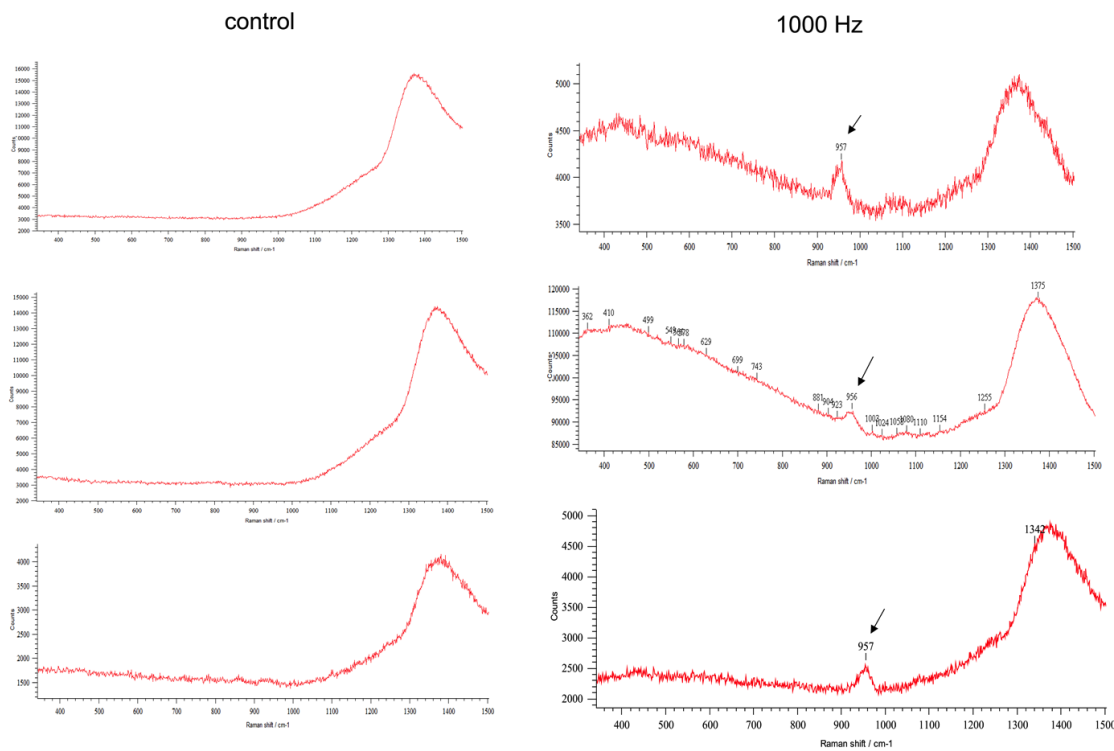
Supplementary Figure 2. Comparison of 2.5 mL and 5.0 mL collagen gel fill on the nanovibration effect. (a&b) Collagen gel interferometric measurements change in displacement (nm) relative to voltage at a particular frequency, measurements performed on the collagen gel surface in a 6 well plate. (a) Assessment performed on a 2.5 mL collagen gel fill. (b) Assessment performed on a 5 mL collagen gel fill. Frequencies assessed were 500, 1000, 2000 and 4000 Hz and mean measurements appeared to be linear across voltages measured i.e. 16, 32, 48, 64, and 80 V (peak to peak). (c to h) Collagen gel interferometric measurements - displacements in nm were measured in 6 well plates, measurements were performed at 80 V for 500, 1000, 2000, 3000 and 4000 Hz. (c) Summary of displacement in nm for a 2.5 mL gel fill (d) Summary of displacement in nm for a 5 mL gel fill. (e) 2.5 mL gel fill measurements for centre only. (g) 2.5 mL gel fill measurements for edges only. (f) 5 mL gel fill measurement for centre only. (h) 5 mL gel fill measurement for edges only. N = 6 measurements for (c-d), and N = 3 measurements for (a-b, e-h).



Supplementary Figure 3. Viability and metabolic activity of MSCs seeded into collagen gels with/without nanovibrational stimulation. A&C are low and high magnification images of live/dead staining (live cells are green, dead cells are red) for MSCs in collagen gels after 14 days of nanovibrational stimulation showing a highly viable cell population. B&D are low and high magnification images of live/dead staining for MSCs in collagen gels with no nanovibrational stimulation after 14 days culture showing a highly viable cell population. Alamar blue metabolic analysis showed that the nanovibration stimulated MSCs had higher activity at 14 days culture compared to unstimulated 3D culture controls. $D=1$, $r=4$, results = mean \pm SD, stats by ANOVA and Kruskal Wallis test where $*=p<0.05$.



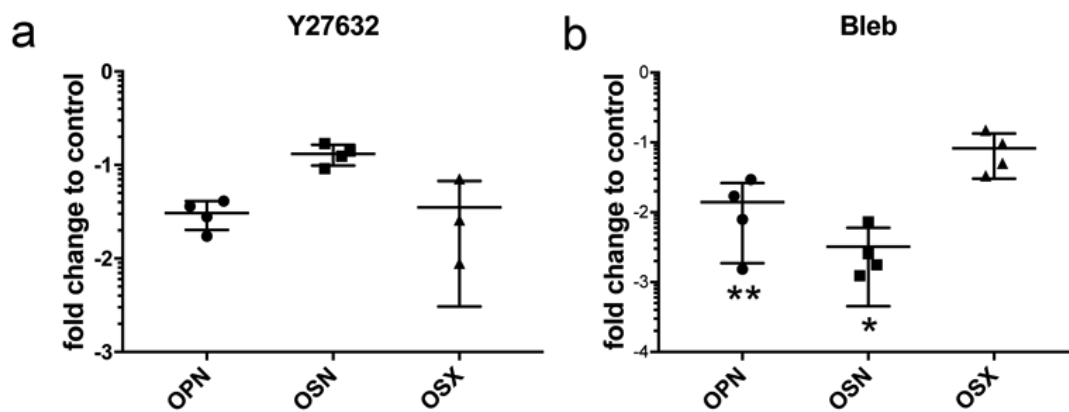
Supplementary Figure 4. Osteogenic assessment of nanovibration on bone protein expression. MSCs exposed to nanovibrations at 1000 Hz for 21 days in 3D assessed against unstimulated controls for quantitative protein expression of osteocalcin OCN using in cell western showing significant increase by nanovibrational stimulation. Seeding = 100,000 MSCs per gel, d=1, r= 6, results are mean \pm SD, ***p< 0.05 by unpaired T-Test.



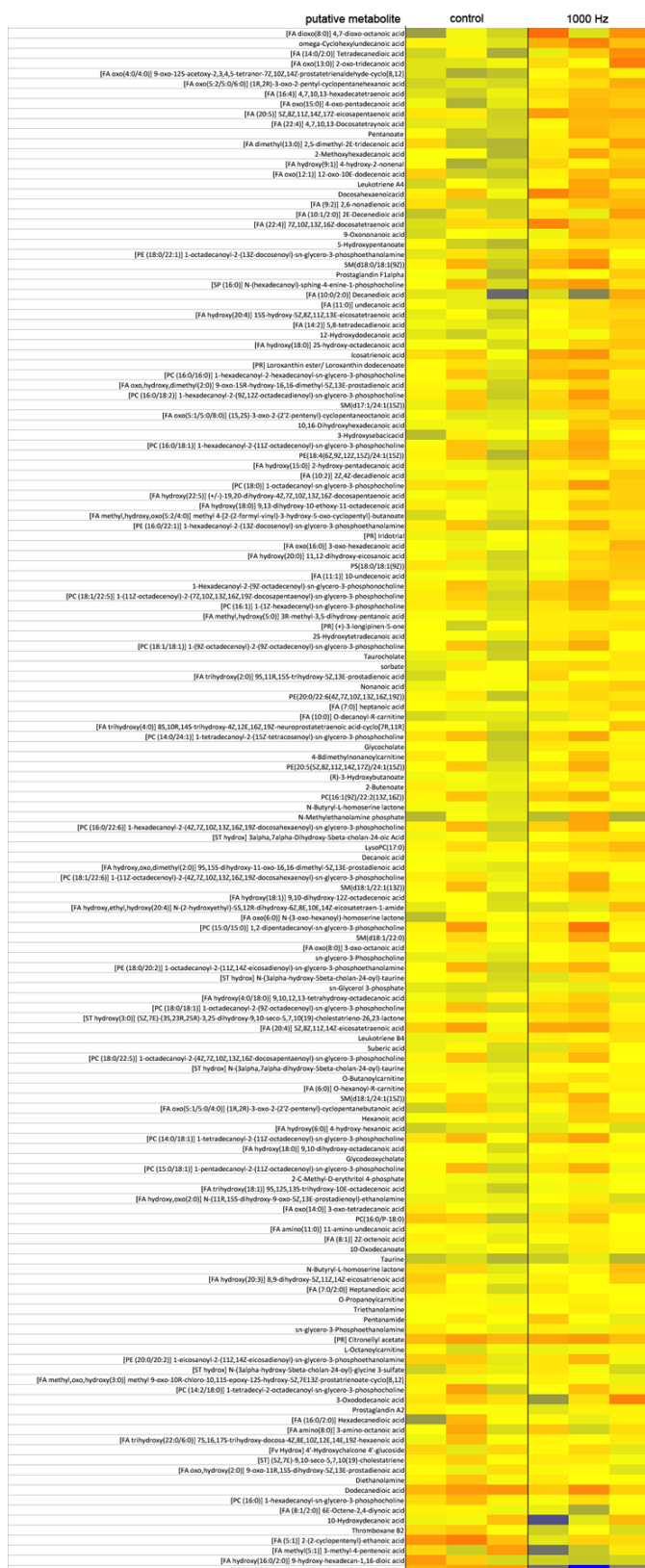
Supplementary Figure 5. Further Raman Spectra. Arrows indicate phosphate peak.

Supplementary table 2. Quantitative results of Raman scattering. Raman spectra results for nanovibrated samples relative to the reference standard of cortical compact bovine mineralised bone. Values are shown for the Raman shift peak height, area and full width at half height maximum (FWHM). The lower the value the greater the crystalline alignment and hence an indication of mineral density^{1,2}.

	Bovine Cortical Bone	1000 Hz (mean value)
Peak Raman Shift	960 cm ⁻¹	960 cm ⁻¹
Height	134510	2260
Area	3.030 x 10 ⁷	2.3 x 10 ⁶
FWHM	16.754	28.495



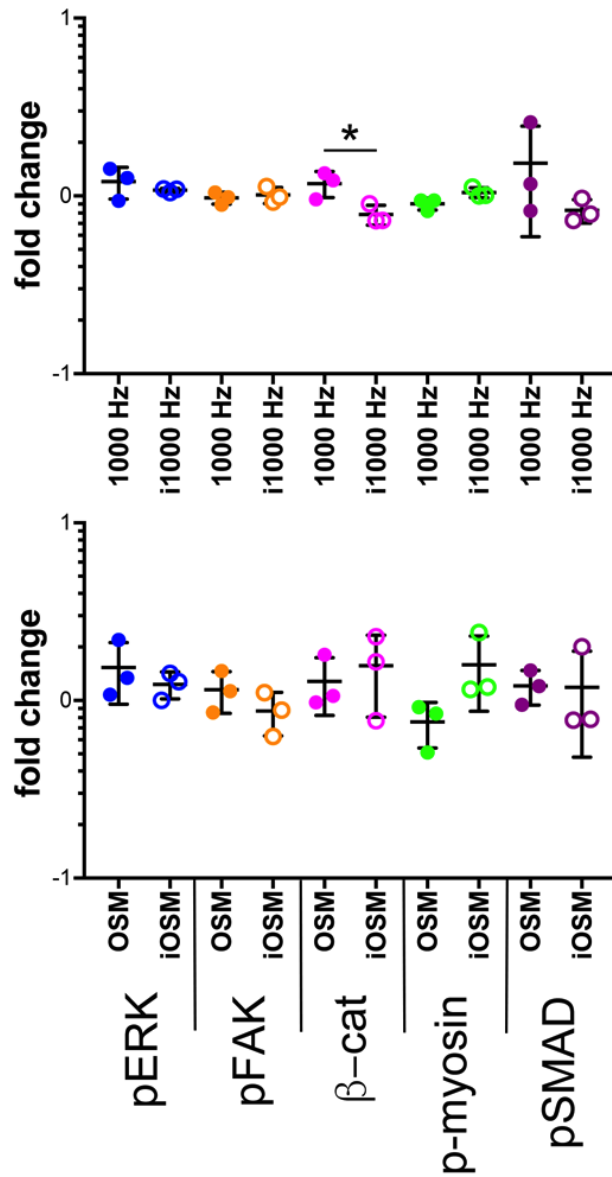
Supplementary Figure 6. Analysis of osteoblast genes at 14 days of culture after inhibition of intracellular tension. Data looking at osteopontin (OPN), osteonectin (OSN) and osterix (OSX) shows down regulation of OPN and OSN with blebbistatin inhibition at this time point. Results are mean \pm SD ($d=1$, $n=4$, $t=2$), stats by ANOVA with Kruskal Wallis and Dunn's post-test where $*=p<0.05$ and $**=p<0.01$. Values are on a log scale.



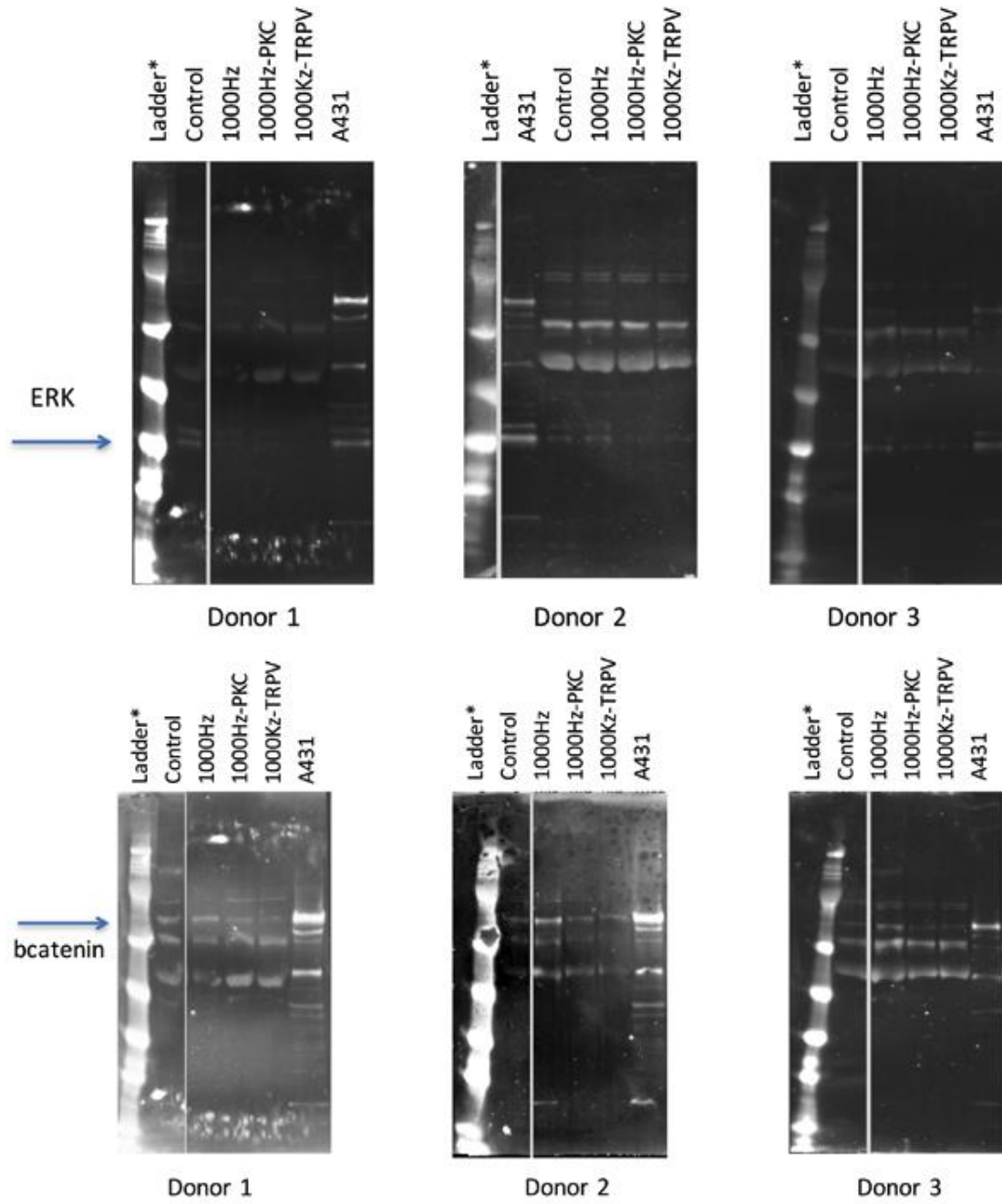
Supplementary Figure 8. Heatmap of lipid metabolism. More up-regulations in the lipid class are seen in MSCs cultures in 3D with nanovibrational stimulation. Red=up, blue = down and yellow = no change. D = 1, r = 3.



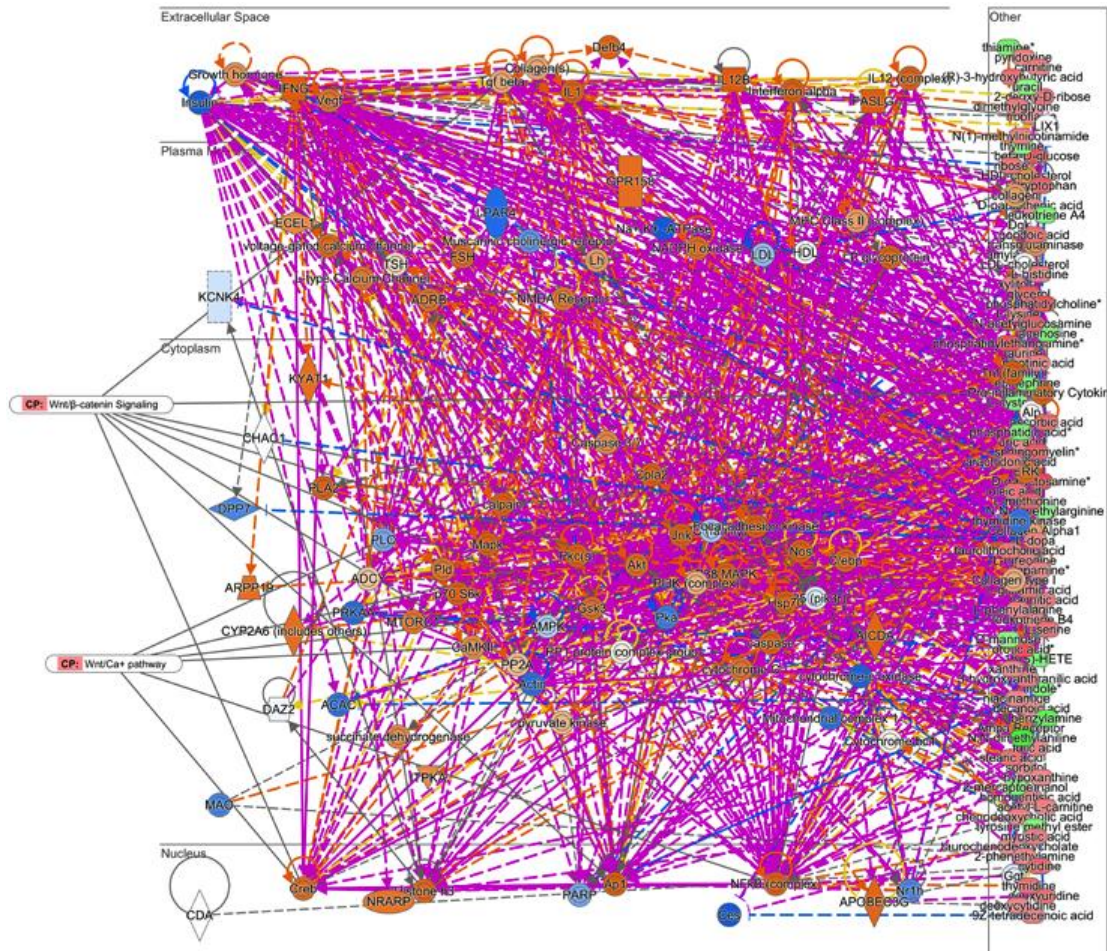
Supplementary Figure 9. Heatmap of carbohydrate metabolism. More up-regulations in the carbohydrate class are seen in MSCs cultures in 3D with nanovibrational stimulation. Red=up, blue = down and yellow = no change. $D = 1$, $r = 3$.



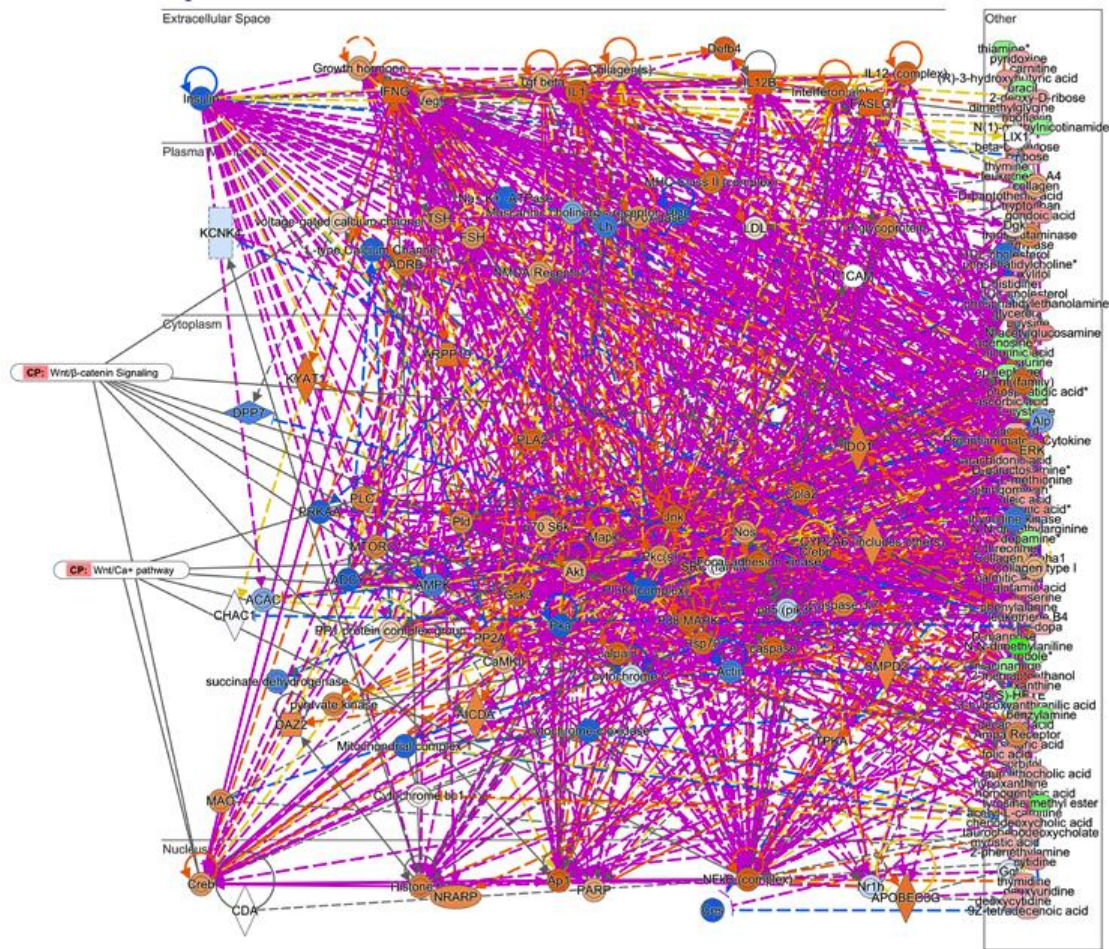
Supplementary Figure 10. Western blot analysis for 3D cultures. (a) Comparison between 3D MSCs with nanovibrational stimulation and with similar treatment but with PKC inhibition (i) showing a decrease in β -catenin. (b) Comparison between 3D control MSCs and with similar treatment but with PKC inhibition (i) showing no significant change. $D=3$, $r=3$ (4 pooled/lane), $*=p<0.05$ by Tukey test. Values are on a log scale.



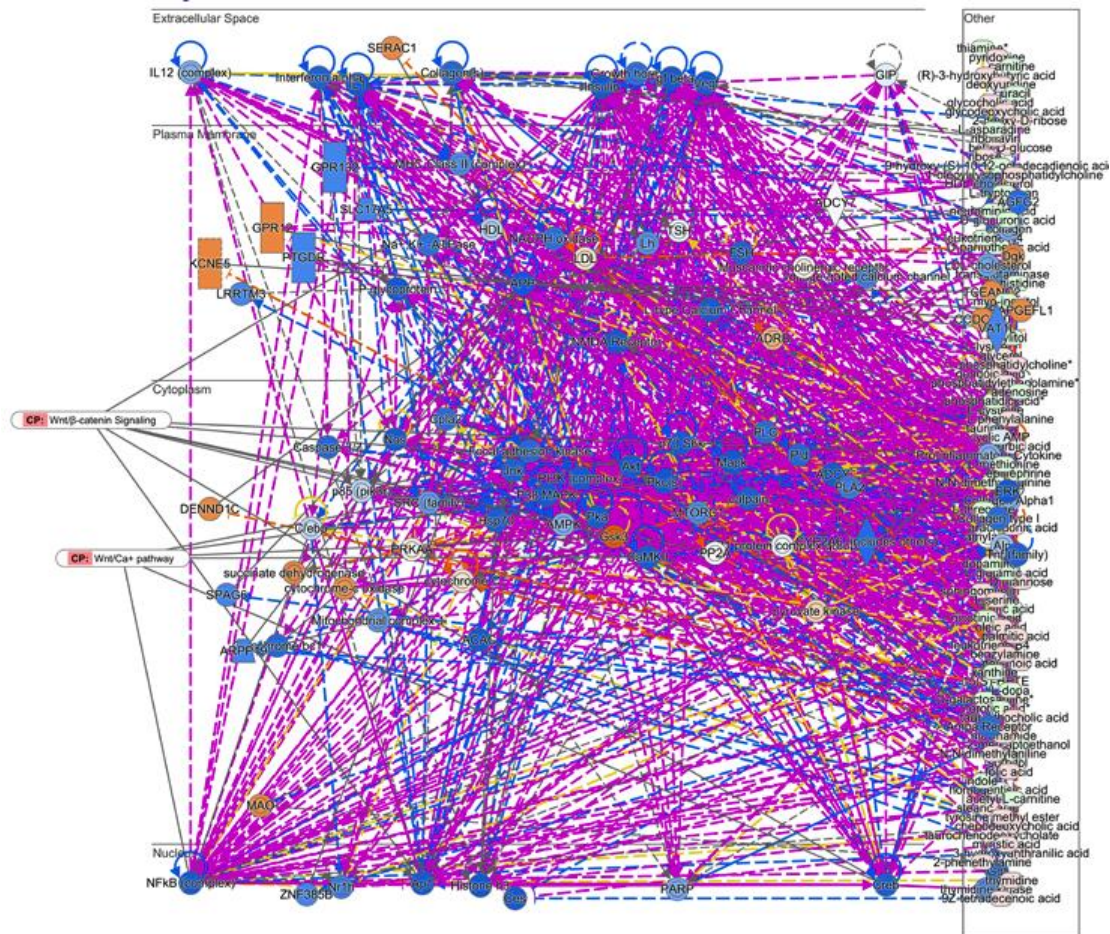
Supplementary Figure 11. Western blots corresponding to Figure 5b.



Supplementary Figure 12. Metabolomics links to wnt signalling for nanovibrationally stimulated MSCs after 5 days of culture. Metabolite changes (left hand side, red=up-regulation, green = down-regulation) leads to a majority of predicted up-regulations (orange = up-regulation, blue = down-regulation) for biochemical hubs feeding into Wnt signalling. $D = 3$, $r = 4$.



Supplementary Figure 13. Metabolomics links to wnt signalling for NS-PKC stimulated MSCs after 5 days of culture. Metabolite changes (left hand side, red=up-regulation, green = down-regulation) leads to more of a balance of predicted up-regulations and down-regulations (orange = up-regulation, blue = down-regulation) for biochemical hubs feeding into Wnt signalling. $D = 3$, $r = 4$.



Supplementary Figure 14. Metabolomics links to wnt signalling for NS-TRPV stimulated MSCs after 5 days of culture. Metabolite changes (left hand side, red=up-regulation, green = down-regulation) leads to a prevalence of down-regulations (orange = up-regulation, blue = down-regulation) for biochemical hubs feeding into Wnt signalling. $D = 3$, $r = 4$.

Supplementary Table 3. RT-PCR Reverse transcription thermal programme.

Temp	Time
42°C	15 min
93°C	3 min
4°C	Hold

Supplementary Table 4. Primers for genes used to perform qPCR.

Gene Name	Forward Primer	Reverse Primer
GAPDH	TCAAGGCTGAGAACGGGAA	TGGGTGGCAGTGATGGCA
Actin	GTGGGCCGCCCTAGGCACCAG	CACTTTGATGTCACGCACGATTC
18s	GCAATTATTCCCATGAACG	GGGACTTAATCAACGCAAGC
RUNX2	GGTCAGATGCAGGCGGCC	TACGTGTGGTAGCGCGTGGC
BMP2	CTTCTAGCGTTGCTGCTTCC	AACTCGCTCAGGACCTCGT
ALP	ATGAAGGAAAAGCCAAGCAG	CCACCAAATGTGAAGACGTG
OPN	AGCTGGATGACCAGAGTGCT	TGAAATTCATGGCTGTGGAA
OCN	CAGCGAGGTAGTGAAGAGACC	TCTGGAGTTTATTTGGGAGCAG
COL1	CCATGTGAAATTGTCTCCA	GGGGCAAGACAGTGATTGAA
OSX	GGCAAAGCAGGCACAAAGAAAG	AATGAGTGGGAAAAGGGAGGG
Osteonectin	AGAATGAGAAGCGCCTGGAG	CTGCCAGTGACAGGGAAGA
BMPR1a	CTACTGACACCAGAGCC	GGTCAGCAATGCAGCAACTC
PIZO1	TCGCTGGTCTACCTGCTCTT	GGCCTGTGTGACCTTGA
PIZO2	CCCGGAGTTTGAAAATGAAG	CAGTGCCTCTTGAATCAATTT
TRPA1	TGGACACCTTCTTCTGCATT	TCTTCTCCATTAGCTCAATTTGG
TRPV1	AGAGTCACGCTGGCAACC	GGCAGAGACTCTCCATCACAC
KCNK4	Biorad assay	qHsaCED0047530
KCNK2	CGCTCAGAACTCCAACCGA	CATGAGGCTGCTCCAATGCT

Supplementary Table 5. Information regarding biological experiment replicate numbers linked to the figures.

Figure	Experiment	Cells from X number of donors	Biological replicates	Technical replicates
1f	qPCR	3	4	2
1g	ICW	1	3	2
1h	ICW	3	4	1
3a	qPCR	1	6	2
3b	Von Kossa	3 (4 week) 1 (6 week)	4 5	1 1
3c	Raman	1	3	1
3d-f	μ CT	1	3	1
4a	qPCR	1	3	2
4b-e	qPCR	3	3	2
4f-h	qPCR	2	4	2
5a	Western	3	4 (pooled)	3
5b	Western	3	4 (pooled)	3
5c-e	Metabolomics	1	3	1
6	qPCR	3	4	2
S3a-d	Live/dead	1	4	1
S3e	Alamar blue	1	4	3
S4	ICW	1	6	1
S6	qPCR	1	3	1
S7&8	Metabolomics	3	4	1
S9	Western	3	4 (pooled)	3

Supplementary references.

1. Tarnowski, C.P., Ignelzi, M.A., Jr. & Morris, M.D. Mineralization of developing mouse calvaria as revealed by Raman microspectroscopy. *Journal of bone and mineral research : the official journal of the American Society for Bone and Mineral Research* 17, 1118-1126 (2002).
2. Gentleman, E., *et al.* Comparative materials differences revealed in engineered bone as a function of cell-specific differentiation. *Nat Mater* (2009).